THREE YEARS OF TRMM PRECIPITATION FEATURES. PART I: RADAR, RADIOMETRIC, AND LIGHTNING CHARACTERISTICS

DANIEL J. CECIL

University of Alabama in Huntsville, Huntsville, AL

STEVEN J. GOODMAN and DENNIS J. BOCCIPPIO

NASA Marshall Space Flight Center, Huntsville, AL

EDWARD J. ZIPSER

University of Utah, Salt Lake City, UT

STEPHEN W. NESBITT

Colorado State University, Fort Collins, CO

Submitted to *Monthly Weather Review*, 26 FEB 2004

Revised, 4 AUG 2004

Corresponding author address: Daniel J. Cecil, Earth System Science Center, University of Alabama in Huntsville, 320 Sparkman Dr, Huntsville, AL 35805. E-mail: Daniel.Cecil@msfc.nasa.gov

Abstract

During its first three years, the Tropical Rainfall Measuring Mission (TRMM) satellite observed nearly six million precipitation features. The population of precipitation features is sorted by lightning flash rate, minimum brightness temperature, maximum radar reflectivity, areal extent, and volumetric rainfall. For each of these characteristics, essentially describing the convective intensity or the size of the features, the population is broken into categories consisting of the top 0.001%, top 0.01%, top 0.1%, top 1%, top 2.4%, and remaining 97.6%. The set of "weakest / smallest" features comprises 97.6% of the population because that fraction does not have detected lightning, with a minimum detectable flash rate 0.7 fl min^{-1}. The greatest observed flash rate is 1351 fl min^{-1}; the lowest brightness temperatures are 42 K (85-GHz) and 69 K (37-GHz). The largest precipitation feature covers 335,000 km^2 and the greatest rainfall from an individual precipitation feature exceeds $2x10^{12}$ kg of water. There is considerable overlap between the greatest storms according to different measures of convective intensity. The largest storms are mostly independent of the most intense storms. The set of storms producing the most rainfall is a convolution of the largest and the most intense storms.

This analysis is a composite of the global tropics and subtropics. Significant variability is known to exist between locations, seasons, and meteorological regimes. Such variability will be examined in Part II. In Part I, only a crude land / ocean separation is made. The known differences in bulk lightning flash rates over land and ocean result from at least two differences in the precipitation feature population: the frequency of occurrence of intense storms, and the magnitude of those intense storms that do occur. Even when restricted to storms with the same brightness temperature, same size, or same radar reflectivity aloft, the storms over water are

considerably less likely to produce lightning than are comparable storms over land.

1. Introduction

The Tropical Rainfall Measuring Mission (TRMM) satellite has collected detailed measurements of rainstorms in the tropics and subtropics since its launch in late 1997. The instrument suite provides simultaneous measurement of many quantities related to precipitation, e.g. radar reflectivity, passive microwave brightness temperature, infrared cloud top temperature, lightning flash rate and location. This combination allows detailed characterization of millions of individual precipitation features.

The characteristics of nearly six million precipitation features are presented here, representing the first three years of TRMM observations. The purpose is to provide a global (tropical and subtropical) context for individual cases and for regional, seasonal, or other regime-dependent studies. Furthermore, we seek to improve the understanding of individual measurable characteristics (e.g., brightness temperature) by exploiting simultaneous measurements of other characteristics (e.g., radar reflectivity profiles and lightning flash rates). The large, comprehensive database enables bulk quantification of relationships between these characteristics, which have previously been examined using idealized models (Vivekanandan et al. 1990, 1991; Skofronick-Jackson and Wang 2000) and/or much smaller sets of storms from particular regions (Shackford 1960; Spencer 1986; Spencer et al. 1989; Dye et al. 1989; Mohr et al. 1996; Toracinta et al. 1996, 2002; Nesbitt et al. 2000; Carey and Rutledge 2000; Petersen and Rutledge 2001; Cecil and Zipser 2002). Many of the relationships presented here are consistent with those reported in previous studies, but the size of this database and the unique combination of radar, radiometer, and lightning sensor allow some analyses (e.g., probability of lightning as a

function of brightness temperature or reflectivity) which would otherwise be less comprehensive or even impossible. Emphasis is placed on the most vigorous and/or largest features, as these have the greatest impact on the hydrologic cycle, latent heating, atmospheric composition, and hazards to humans.

The main objective of the paper is a quantitative description of the three-year database, over all locations and seasons, describing the full spectrum of precipitation features. This includes quantification of storm properties which are (i) *necessary* or (ii) *typical* for storms of varying flash rates and for storms of varying brightness temperatures. This can be used to evaluate radiative transfer models or parameterizations based on lightning, brightness temperature, or radar reflectivity information.

Precipitation features are identified as contiguous rain areas using the algorithm of Nesbitt et al. (2000). Each precipitation feature's size is recorded, as are each feature's total rainfall and several measures of convective intensity (lightning flash rate, minimum brightness temperatures, vertical profile of maximum radar reflectivity). Section 2 describes the measurement and interpretation of these characteristics, and introduces a categorization of the precipitation features based on the magnitudes of these individual characteristics. The three-year population of precipitation features is summarized by relative and cumulative frequency distributions for each characteristic in Section 3. The characteristics are intercompared in Section 4, with example precipitation features presented. Section 5 summarizes and discusses the findings. The frequency distributions and the relationships of individual characteristics with each other vary greatly between regions / seasons / convective regimes. This is crudely addressed (in Section 3 only) by separating the precipitation features into those over land and those over water. Part II of this

study will examine such variability in greater detail, including geographic and temporal distribution of the precipitation features.

2. Data and Methods

a. Instrumentation and sampling

The database consists of simultaneous observations from the Precipitation Radar (PR), TRMM Microwave Imager (TMI), and Lightning Imaging Sensor (LIS) aboard the TRMM satellite. Instrument and data characteristics are summarized below. For greater detail, PR and TMI are described by Kummerow et al. (1998; 2000); LIS is described by Christian et al. (1999) and Boccippio et al. (2002). Version 5 PR and TMI data and Version 4 LIS data are used in this study, all collected prior to the August 2001 TRMM satellite altitude boost.

The PR is a 13.8 GHz radar with a 220 km wide swath. Pixel spacing is very nearly the same as the footprint size (4 km), with virtually no overlap or undersampling. We focus on reflectivities at least 20 dBZ, which is safely above the minimum detectable (~17 dBZ - Kozu et al. 2001). The standard TRMM attenuation corrected reflectivity product (2A25) is used.

The TMI is a conically scanning radiometer viewing earth's surface at a 49° nadir angle. This study uses polarization corrected temperature (PCT) at 85-GHz (Spencer et al. 1989) and 37-GHz (Cecil et al. 2002). This removes the sharp gradient between land and ocean surfaces, allowing precipitation over either surface to be treated consistently. For large optical depths, the polarized brightness temperatures and the PCT are nearly equal.

The TMI footprint sizes are 7x5 km (85-GHz) and 16x9 km (37-GHz). These match the pixel spacing in the across scan direction. Successive scans are 14 km apart, resulting in undersampling at 85-GHz and oversampling at 37-GHz.

LIS is a staring optical imager, detecting rapid changes in the background scene. Spatial, spectral, and temporal filters determine whether these changes are associated with lightning. The oxygen emission multiplet at 777.4 nm is monitored, allowing detection of lightning during both daytime and nighttime conditions. Horizontal resolution is ~5 km and a location is usually observed for ~80 s during a satellite overpass. One flash in 80 s allows a minimum detectable flash rate of 0.7 fl min^{-1}. Detection efficiency is estimated to be about 85% (Boccippio et al. 2002). *Detection efficiency is not accounted for when computing flash rates in this study.*

The TRMM satellite orbits with a 35° inclination angle. The number of samples rapidly increases at the highest latitudes, with the 35° zone seen roughly twice as often as equatorial regions.

b. Precipitation feature database

A three-year (December 1997 through November 2000) precipitation feature database was developed by Nesbitt and Zipser (2003), using the Nesbitt et al. (2000) algorithm. Precipitation features are defined as contiguous areas having at least 20 dBZ near surface reflectivity *or* having 85-GHz PCT ≤250 K. This generally corresponds to the area experiencing rain at the surface, but the 85-GHz scattering criteria also includes thick ice clouds which may not be raining at the surface. The minimum size is ~75 km^2 (four PR pixels). Large features are limited by the size of the PR swath, with the largest features covering ~10^5 km^2. These are rain systems which range from meso-gamma to meso-alpha scale and often contain multiple convective cells.

Each lightning flash is matched to its nearest TMI pixel. The flashcount is summed and the viewtime is averaged over the set of TMI pixels comprising a precipitation feature. In some cases an unexpectedly low flashcount is explained by a large number of flashes *near* the precipitation

feature. This may be due to inconsistencies from parallax, sensor geometry, or actual displacement of the lightning activity from the surface precipitation field[1].

c. Categorization of precipitation features

Several parameters are saved describing each precipitation feature. These include size, volumetric rainfall, total area meeting certain convective thresholds, and point measures of convective intensity. The point measures (minimum 85- and 37-GHz PCT, maximum reflectivity as a function of altitude) are meant to represent the strongest convection within the borders of the precipitation feature. This study adds lightning flashcount and viewtime (and hence flash rate) to the list of parameters for each feature. Also, the vertical reflectivity information has been converted to a temperature coordinate, using NCEP environmental conditions for each precipitation feature. This yields a vertical profile of maximum reflectivity at temperature levels 0 through –60° C.

Lightning depends on collisions between large ice and smaller ice in the presence of supercooled liquid water (Takahashi 1978; Saunders and Peck 1998), so the local flash rate depends on the vigor of convection and upward fluxes of water in the mixed phase region. Precipitation feature flash rate is a convolution of both this local convective intensity and the areal coverage of deep convection. Precipitation feature minimum brightness temperatures depend on the optical path of large (hundreds or thousands of micron) ice at 85- and 37-GHz. This is similar to a column-integrated ice mass, weighted toward the larger particles (especially at 37-GHz, with its longer wavelength) (Vivekanandan et al. 1991). Emission and scattering by liquid water also contribute to the signal at these frequencies. The minimum brightness

[1] For example, a few flashes are displaced east of the convective core in Fig. 11.

temperature generally represents the deepest, most vigorous convection in the storm. The maximum reflectivity parameters depend on the size, phase, and concentration of the largest precipitation particles at specific vertical levels in the mixed phase region, again representing the most vigorous local convection in the precipitation feature. For multicell storms, these minimum brightness temperature and maximum reflectivity measurements are not required to represent the same cell, but in practice they do tend to be located close to one another and close to the lightning flash density maximum.

Precipitation feature size (total area) is another of the stored parameters. This is essentially the horizontal extent of a continuous rain field. A separate size parameter is the area having 85-GHz PCT $\leq$150 K. The areal extent of brightness temperatures below this threshold indicates how broad an area is experiencing strong, deep convection (instead of merely experiencing rain or weaker convection). Volumetric rain is based on the 2A25 near surface rain product, integrated over the horizontal extent of the precipitation feature. This total surface rain flux can be expressed in mm h^{-1} km^2 or equivalently 10^6 kg h^{-1}.

Those parameters which are essentially point measures are most useful for topics such as identifying severe storms (e.g., large hail) or for identifying the extremes of what a model should reproduce or take into account. For purposes such as estimating total rainfall, integrated quantities such as total precipitation feature area are more useful. For other purposes such as estimating lightning and related quantities, an integrated area of deep convection may be more useful. For example, Marshall and Radhakant (1978) related lightning sferics rates to the total area having at least 30 dBZ radar reflectivity at 6 km altitude. One advantage of compiling the maximum and minimum point measures is that it facilitates comparison of measurables which

respond to related geophysical parameters, but do not share identical measurement footprints.

For any parameter, the population of precipitation features is divided into six categories (CAT-0 – CAT-5) in order to differentiate the qualities of the extraordinary systems (Table 1). CAT-0 ("weak") comprises the bottom 97.6% (by size, or by flash rate, or by minimum 85-GHz PCT, etc.) of the population. This corresponds to the fraction of precipitation features in which LIS does not detect lightning. This includes some features which may have lightning, but it goes undetected while the feature is observed during a gap between flashes. Similarly, some features with observed lightning certainly have flash rates less than the nominal 0.7 fl min^{-1} detectable during 80 s of observation. Some are simply observed at the right time that lightning does occur. Statistically, 97.6% represents the portion of precipitation features having flash rates less than the minimum detectable.

The populations reaching thresholds for CAT-2 ("strong"; top 1.0%) through CAT-5 ("extreme"; top 0.001%) differ by an order of magnitude per category. The categories are defined separately for any parameter. For example, there are 58 CAT-5 lightning storms, but these are not the same 58 storms reaching CAT-5 for precipitation feature size, brightness temperature, reflectivity, etc.

3. Overview of the Precipitation Feature Population

For any of the precipitation feature properties examined here, the vast majority of precipitation features are small and/or weak. This is demonstrated by the probability density functions and cumulative density functions in Fig. 1, 3-8. Note the logarithmic axes in these plots. The land and ocean curves are based on whether the majority of pixels in a precipitation

feature are located over a landmass or a body of water. This is only a crude land/ocean separation with some errors; more careful analysis will be presented in Part II of this study.

a. Lightning flash rate

The most common lightning flash rate is zero; 97.6% of the precipitation features do not have lightning detected by LIS. That is, the cumulative density function (thick solid line in Fig. 1a) intersects the y-axis at 2.4×10^{-2}. Additionally, the most common non-zero flash rate is the minimum detectable. The probability density function (thin solid line in Fig. 1a) shows that 1% of the precipitation features have ~1 fl min^{-1}. Some of the 0 fl min^{-1} storms are likely electrically active, but having flash rates too low to be reliably detected. Extrapolation of the cumulative density function to lower flash rates (Fig. 1b) suggests that up to ~10% of the features may have lightning. Several hundred flashes per minute are observed in the greatest flash rate storms, with one storm in the three-year database exceeding 1000 fl min^{-1}. These are large mesoscale convective systems (MCS) with contributions from intense individual convective cells or lines.

Even among the precipitation features with lightning detected by LIS (Fig. 1c), most flash rates are relatively low by LIS detectability standards. Half of them are 2 fl min^{-1} or less (where the thick solid line reaches 5×10^{-1} in Fig. 1c), and 85% are below 10 fl min^{-1}. Only 0.7% exceed 100 fl min^{-1}. On the other hand, the rarity of LIS-detected lightning in the precipitation feature database suggests that even a few flashes per minute may be a "hi gh" flash rate.

The occurrence of lightning is an order of magnitude more common in precipitation features located over land (10%; where the thick dashed line intersects the y-axis in Fig. 1a) than in those located over water (1%; where the thick dotted line intersects the y-axis in Fig. 1a). Among precipitation features with detected lightning, there is still at least a factor of two difference

between continental and oceanic flash rates (Fig. 1c). The difference is even greater than that shown in Fig. 1c, because many of the high flash rate "oceanic" storms are actually along coasts.

The precipitation features with observed lightning are mapped in Fig. 2. Different symbols and colors are used for each flash rate category (CAT-1 through CAT-5). The lowest observed flash rates (CAT-1-2) occur virtually everywhere that precipitation features in general are abundant, but they occur more frequently over land than over ocean. The highest flash rate storms (CAT-4-5, with at least 122 fl min^{-1}) occur almost exclusively over land or just east of subtropical continental locations (downflow from land masses and over warm, poleward-moving ocean currents). The subtropical Americas produce the greatest spatial density of these highest flash rate storms. Central Africa is the only location in the deep tropics where more than a few of them occur. More thorough analysis of the geographical and seasonal distribution of precipitation features by flash rate (and by the other parameters) is reserved for a subsequent analysis beyond the scope of this paper.

b. Minimum 85- and 37-GHz brightness temperature

Brightness temperatures similar to a rain-free background (>275 K) are most common (Fig. 3a, 4a). Only 13% of precipitation features have minimum 85-GHz PCT 250 K or less, which is used as a threshold[2] to indicate ice scattering consistent with moderate rain (Spencer et al. 1989). Only 6% achieve the 225 K threshold at 85-GHz used by Mohr and Zipser (1996) to identify

[2] This threshold in the precipitation feature algorithm accounts for the discontinuity in the probability density function at 250 K, with 63000 precipitation features triggered by the 250 K criteria but failing to reach the 20 dBZ criteria. Some of these are likely mis-identifications due to surface snow cover, which has a low microwave emissivity. These do not include 36000 precipitation features which have been pre-filtered from the database due to surface snow contamination.

deep convection in an MCS. About 5% have 37-GHz PCT below 265 K, a rough threshold for 37-GHz ice scattering (as opposed to reduced PCT due to emission). The lowest brightness temperatures are well below 100 K at 37-GHz and below 50 K at 85-GHz, indicating very large (several cm) hail.

The frequency distribution of brightness temperatures for the overall population of precipitation features is sharply peaked at high TB, especially for oceanic precipitation features. Very low brightness temperatures due to strong ice scattering are about an order of magnitude more common in precipitation features over land than over ocean (Fig. 3a, 4a). The brightness temperature distributions for features with detected lightning are very broad (Fig. 3b, 4b). At 85-GHz, there are roughly equal numbers of features with lightning for brightness temperatures ranging from ~150 K to ~225 K. There is a slight tendency for the oceanic thunderstorms to have lower brightness temperature (~150 K at 85-GHz), while more continental thunderstorms have brightness temperatures greater than 200 K.

While precipitation features in general become less common as brightness temperature decreases, the likelihood that a given feature produces lightning rapidly increases (Fig. 3c, 4c). Only 2% of the features with 250 K minimum 85-GHz PCT have lightning. One quarter of the features with 200 K minimum 85-GHz PCT have lightning, and nearly half of the features with lower brightness temperatures have lightning. However, only 3% of the precipitation features have such low brightness temperatures. These percentages include dramatic land-ocean differences. For 200 K at 85-GHz, about 10% of oceanic precipitation features produce lightning but more than half (58%) of the continental precipitation features produce lightning. The trends at 37-GHz are similar, except a smaller dynamic range is realized (Fig. 4). The land-ocean

differences are less dramatic at 37-GHz, but still substantial.

c. Size

The smallest features are most common - 21% of the features have only the minimum four pixels (74 km^2) (Fig. 5a). More than half of the features have seven or fewer pixels (130 km^2). The largest precipitation features cover ~10^5 km^2. These extensive areas of contiguous rainfall sometimes include multiple MCS. The largest features extend beyond the PR swath; thus their true sizes (and sometimes their intensities) are underestimated.

The smallest precipitation features usually do not have lightning detected by LIS. The most common size of features with lightning is ~300 km^2 (Fig. 5b), but only 2% of all features this size have detected lightning (Fig. 5c). There is only a weak relationship between precipitation feature size and whether or not lightning occurs. The probability of lightning increases slowly with feature sizes up to ~30000 km^2. About 30% of features this large have lightning, but that fraction decreases for larger precipitation feature sizes.

d. Areal extent of intense convection; volumetric rain

Similar plots showing the relative frequency distributions of precipitation features according to their total area experiencing intense convection (85-GHz ≤150 K) and their volumetric rain are presented in Fig. 6-7. These distributions are somewhat similar to those for measures of convective intensity (e.g., minimum TB) and precipitation feature size, respectively, although both of these measures represent a combination of convective intensity and areal coverage. One notable difference is that the probability of lightning increases monotonically with both area experiencing intense convection (Fig. 6c) and volumetric rainfall production (Fig. 7c), whereas it decreases with precipitation feature size among the largest features (Fig. 5c). The very largest

precipitation features in Fig. 5 often consist of vast areas of light to moderate rainfall; therefore, many of them do not produce detectable flash rates or the most extreme volumetric rainfall totals.

e. Vertical profile of maximum radar reflectivity

Considering each precipitation feature's maximum reflectivity as a function of height (temperature), the median value near the surface is 33 dBZ. At the freezing level, the median is only 22 dBZ. At higher altitudes, most precipitation features do not have detectable reflectivity. Only ~10% have measured reflectivity at the –30° C level, and ~1% have at least 30 dBZ at this level (Fig. 8a). The reflectivities aloft tend to be much greater for precipitation features over land than for those over water (Fig. 8b). At the freezing level, the median land profile is 8 dB greater than the median ocean profile. At the –30° C level, 1% of the features over land measure at least 40 dBZ, but more than an order of magnitude fewer features over water reach this threshold. This is consistent with differences in flash rate and ice scattering signatures over land and over water.

Because lightning generally requires a well-developed mixed phase region, the precipitation features which produce lightning do have significant reflectivity aloft. The median reflectivity among this subset is 40 dBZ at –10° C and 30 dBZ at –30° C (Fig. 8c). The median profiles of maximum reflectivity are nearly identical for thunderstorms over land and over water (Fig. 8d). The strongest thunderstorms over land (as indicated by their reflectivity profiles) tend to have greater reflectivities than the strongest thunderstorms over water. More than 10% of thunderstorms over land reach 40 dBZ at –30° C; less than 5% of those over water reach this threshold.

This database demonstrates the importance of having a large ice mass *in the mixed phase*

region in order for lightning to occur. One in four features having 50 dBZ reflectivity at the freezing level do not have LIS-detected lightning (Fig. 8e). These cases are likely dominated by warm rain processes, with significant ice microphysics not yet established. When the 50 dBZ echo reaches –20° C or colder, on the other hand, it is virtually guaranteed that the precipitation feature is producing lightning. For weaker reflectivities, ~90% of features with 40 dBZ at –20° C and ~25% of features with 30 dBZ at –20° C have detected lightning. This also has a considerable land-ocean difference, as 42% of the features over land have lightning when the reflectivity is 30 dBZ at –20° C, but only 13% of such storms over water have lightning (Fig. 8f).

With the 0.7 fl min^{-1} threshold for detectability, 30 dBZ at the –30° C level can be identified as a threshold at which half of the storms produce lightning and half do not (Fig. 8e). Such thresholds restricted to over-land and over-water cases are 27 and 32 dBZ, respectively (Fig. 8f). A similar threshold is 40 dBZ at -10°C (37 dBZ over land and 41 dBZ over water), with 50% probability of lightning in Fig. 8e (8f).

Dye et al. (1989) identified 40 dBZ at –10° C as a threshold at which rapid electrification occurred in two small New Mexico thunderstorms. Buechler and Goodman (1990) added cases from Alabama and Florida, with this threshold identifying all of the thunderstorms and having a false alarm rate of 20% (7% when restricted to storms with at least 9 km echo tops). Gremillion and Orville (1999) considered reflectivities at 5 dB intervals, examining airmass and sea breeze thunderstorms near Cape Canaveral, Florida. They found optimal thresholds for identifying cloud-to-ground lightning at 40 dBZ (-10° C), 30 dBZ (-20° C), and 20 dBZ (-20° C). Most storms produced their first cloud-to-ground flashes within several minutes of reaching these thresholds. Michimoto (1991) similarly identified a threshold of 30 dBZ at -20° C for

thunderstorms observed in Japan. As these researchers have noted that their thresholds may not apply to other regimes, we note that Fig. 8e-f represent averages over the global tropics and subtropics. It is also important to note the limited duration of LIS observations (~80 s) in Fig. 8, yielding an effective minimum flash rate 0.7 fl min^{-1}. Many low flash rate storms would not be detected by LIS; furthermore, the literature cited above focuses on thresholds which *precede* the occurrence of lightning.

4. Multi-parameter perspective

In this section, we examine how the precipitation feature properties vary with each other. For example, the 58 most extreme storms determined by one property are not necessarily the same 58 CAT-5 storms determined by another property. How do they relate? This is addressed by Tables 2a-f and subsequent figures.

a. Categorization by flash rate

Initially we examine median values for each category. In Fig. 9, the large numerals indicate median vertical profiles of maximum reflectivity for the different categories of lightning storms. The typical profile for a feature without LIS-detected lightning (CAT-0) has 32 dBZ near the surface and 22 dBZ near the freezing level, with reflectivity rapidly decreasing below detectability limits above the freezing level. The typical profile for low flash rate thunderstorms (CAT-1; up to 2.2 fl min^{-1}) has much greater reflectivity, with 47 dBZ near the surface, 44 dBZ at the freezing level, and 31 dBZ at –20° C. The typical profiles for higher flash rate storms exhibit progressively greater reflectivities and less rapid decreases of reflectivity with height, consistent with previous studies (Shackford 1960). There is considerable overlap between categories (as indicated by the smaller italicized numerals in the figure, which bound the range of

reflectivities encountered in each category).

The reflectivity profiles in Fig. 9 are consistent with the brightness temperatures associated with each flash rate category (Table 2a). The CAT-0 features (without LIS-detected lightning) mostly have high brightness temperatures (median around 280 K) similar to a rain-free (or warm rain) background. The median brightness temperatures are progressively lower for increasing flash rates. The maximum brightness temperatures are also progressively lower as flash rate increases. This suggests rough thresholds for how strong the ice scattering must be in order for storms to produce given flash rates: *all* of the CAT-4 flash rates have 85-GHz PCT below 183 K and 37-GHz PCT below 239 K; *all* of the CAT-5 flash rates have 85-GHz PCT below 109 K and 37-GHz PCT below 202 K.

A similar relationship does not exist for the *minimum* brightness temperatures listed in each flash rate category. Categories two through five all include storms with 85-GHz PCT below 50 K and 37-GHz PCT below 110 K. These brightness temperatures easily satisfy the CAT-5 ice scattering criteria in Table 1. The extreme convection associated with such low brightness temperatures is always accompanied by several lightning flashes. Whether this means tens or hundreds of flashes per minute depends partly on how broad an area is experiencing intense convection in the precipitation feature. Most CAT-4-5 flash rate storms have well over 1000 km^2 with the 85-GHz PCT depressed below 150 K (Fig. 10). The few storms with CAT-5 37-GHz scattering (< 135 K) but only CAT-2-3 flash rate in Fig. 10 tend to have a smaller area experiencing intense convection.

An example of this can be seen by comparing Fig. 11 with Fig. 12. Fig. 11 shows a 26 fl min^{-1} (CAT-2) storm over India. This is a fairly large storm, with 4300 km^2 (CAT-1 size) inside the

precipitation feature and 1100 km^2 (CAT-3 area with strong convection) having 85-GHz PCT below 150 K. Its true area is larger and its flash rate would qualify as CAT-3 if the flashes outside the PR swath were included. There is only one extreme convective core, and its microwave scattering and reflectivity characteristics almost all rank as CAT-5. Most of the lightning flashes are clustered around this single core. It should be noted in this and subsequent cross-sections that the radar, 85-GHz, and 37-GHz footprints correspond to different sample volumes. They are plotted here by taking the TMI footprints which are located closest to the radar cross-section.

Fig. 12 shows the highest flash rate storm in this three-year database. Note the much larger map scale than in Fig. 11. Besides having the greatest flash rate, this is the largest precipitation feature in terms of area experiencing strong ice scattering (20000 km^2 with 85-GHz below 150 K). Its total size ranks as CAT-4 (127000 km^2). Its ice scattering ranks as CAT-5 for both 85- and 37-GHz; its maximum reflectivity ranks as CAT-3-4. Around 900 flashes are observed, clustered around the *several* cells in the line. The LIS data buffers were overloaded, resulting in a mean viewtime of only 40 s. This often happens with the highest flash rate storms; the example in Fig. 12 is a worst-case scenario. As with the previous example, this storm extends beyond the PR swath and would have a slightly greater size and flash rate if completely sampled.

Table 2a and Figure 9 also reveal that some storms with no LIS-detected lightning do have intense convection as measured by the radar and radiometer. Some of these cases actually have lightning, but it is located outside the precipitation feature boundary (just as some of the lightning in Fig. 11 is located outside the precipitation feature boundary). Similarly, a few low-

reflectivity, high-brightness temperature features are counted as having lightning that could be more appropriately attributed to adjacent storms.

Disregarding such cases from Table 1a, the lowest 85-GHz PCT in what appears to be a *credible* no-lightning feature is 82 K (CAT-3); its minimum 37-GHz PCT is 225 (CAT-2); it has reflectivity greater than 35 dBZ up to the –45° C level (CAT-2 reflectivity throughout the 0 - -60° C layer) (Fig. 13). The lowest 37-GHz PCT in what appears to be a credible no-lightning feature is 204 K (CAT-3). Such strong ice scattering and high reflectivity through the mixed phase region is normally accompanied by tens of flashes per minute.

It is possible that these and other storms did in fact have lightning that went undetected by LIS. Detection efficiency decreases during the daylight (Boccippio et al. 2002 Figs. 5, 9). Other factors are discussed by Boccippio et al. (2002). However, the specific examples noted above occurred at night with the instrument operating nominally. It is possible that the satellite happened to encounter a short-term lull in the flashing, with lightning occurring before and after the ~80 s LIS observation. Some of the storms may be in mature stages in which electrical charging is slow but the abundant precipitation mass has not yet fallen out. There is also a tendency for the intense convection, no-lightning cases to be small features in the vicinity of other storms with lightning. For example, the small precipitation feature near the left of Fig. 14 has no detected lightning, but the storms farther east and south do have lightning. Such cases may be young convective cells that eventually produce lightning, but in which sufficient charge separation has not yet occurred.

The precipitation features without detected lightning (CAT-0) contribute 69% of the total rain produced by all precipitation features (Table 2a). Again, this certainly includes

thunderstorms with flash rates too low to be reliably detected. The 1% of storms with greatest flash rates (CAT-2-5; > 2.2 Fl min^{-1}) contribute 90% of the lightning flashes but only 21% of the total rainfall. Almost half of the lightning and 15% of the rainfall comes from intermediate (CAT-2; 2.2-31 Fl min^{-1}) flash rate storms. The top 0.01% of storms produce 1/8 of all flashes but only 1.4% of total rainfall.

b. Categorization by minimum brightness temperature

The median reflectivity profiles are shaped a bit differently for categories defined by minimum 85-GHz PCT (Fig. 15) instead of by flash rate. As with lightning, the reflectivities are greater (and decrease less rapidly with height) for the stronger 85-GHz storms. However, the slope of reflectivity with height is not as constant for this 85-GHz stratification as it is for the flash rate stratification. Between roughly the freezing level and -40° C, the median profiles based on flash rates have greater reflectivity than the median profiles based on 85-GHz. The minimum profiles have greater reflectivity at high altitude but lesser reflectivity at low altitude in the 85-GHz plot (compared to Fig. 9). These characteristics suggest the 85-GHz parameter has a greater sensitivity to high-altitude ice mass, while lightning production has greater sensitivity to the mixed phase region.

Some comparisons in Table 2b point out differences between a localized convective intensity (represented by minimum 85-GHz PCT) and a horizontally integrated quantity such as flash rate, total area, or volumetric rain. Among CAT-2 85-GHz storms, the median flash rate is only 2 flashes per minute. Even among the CAT-5 storms, with 85-GHz PCT 57 K or less, there are some rather small storms which only rank as CAT-0 or 1 in terms of total area or volumetric rain.

Some high flash rate storms occur with relatively high minimum 85-GHz PCT (75 flashes

per minute in a CAT-0 85-GHz storm; 146 flashes per minute in a CAT-1 85-GHz storm). These tend to be storms over desert regions (especially the Thar Desert in India and Pakistan), where emission by the surface is much greater than normal. The actual brightness temperature depression in such storms is greater than that in a normal CAT-0 or CAT-1 storm. Such situations could pose a problem for TMI-based retrievals. The Version 6 TMI 2A12 algorithm (McCollum and Ferraro 2003) would not account for this warm desert background, although the Version 5 2A12 algorithm would account for this to an extent by comparing the 85 GHz channel (ice scattering) to the 22 GHz channel (background emission).

The CAT-3, 4, and 5 lightning storms with relatively high 85-GHz PCT in Fig. 16 also have relatively low 37-GHz PCT (compared to other features with the same 85-GHz PCT). That is, the high flash rate storms are shifted toward the right of the general population (toward higher 85-GHz PCT) in the 85-37-GHz parameter space (Fig. 16). Some differences between 85- and 37-GHz PCT in these storms may have to do with the transition from Rayleigh scattering to Mie scattering as the hydrometeor size approaches the wavelength of the radiation. The scattering efficiency increases less rapidly with particle size in the Mie regime, as the scattering cross-section oscillates toward a geometric value (hydrometeor size to the second power instead of the sixth power). Although purely speculative, the differences may also result from emission by supercooled cloud and rain water offsetting some of the 85-GHz scattering and enhancing the conditions for charge separation.

The MCS in Fig. 17 has 123 fl min^{-1} (CAT-4) associated with multiple distinct cells, but the greatest flash rate density is associated with the cell near 151 E (on the right in the radar cross-section). This cell has its 37-GHz PCT scattered to 170 K (CAT-4), but its 85-GHz PCT is only

reduced to 118 K (CAT-2). Such a low 37-GHz PCT is normally associated with 85-GHz PCT below 90 K (Fig. 16). In the radar cross-section, we see high reflectivity (>40 dBZ) within 2 km of the top of the radar echo for this cell. Perhaps this convective core includes supercooled liquid water emitting radiation at high altitudes, with only a relatively thin depth of scatterers above it. Modeling studies suggest that such emission from supercooled liquid has a greater impact on the 85-GHz channel than on the 37-GHz channel (Adler et al. 1991; Smith et al. 1992). The spatial offset between the reflectivity core and the scattering core may also be related to the differing sample volumes for each measurement. Recall that the 37 GHz footprint is nearly a factor of 8 larger than the radar footprint, and has a different viewing angle and different pixel centroid.

The presence of low 37-GHz brightness temperatures without correspondingly low 85-GHz brightness temperatures in CAT-0-1 is complicated by snow contamination. The features having the several lowest 37-GHz PCT among CAT-0 85-GHz storms are suspicious, although they survived our initial filters for snow contamination.

The shapes of the median reflectivity profiles defined by minimum 37-GHz PCT (Fig. 18) are similar to those defined by flash rate. The CAT-1 and 2 reflectivities are slightly greater for the flash rate stratification, while the CAT-4 and -5 reflectivities are greater for the 37-GHz stratification. This is especially true above the $-15°$ C level. This may be explained by the fact that minimum 37-GHz PCT is essentially a point measure, but precipitation feature flash rate is integrated over a large area. An extreme 37-GHz PCT requires a localized extreme ice mass (high reflectivity aloft), but an extreme flash rate can be contributed by a larger area of less intense convection.

An intriguing aspect of Table 2c is that some storms apparently have tremendous 85-GHz

scattering without substantial 37-GHz scattering. For example, one CAT-0 37-GHz storm has its 85-GHz PCT scattered as low as 105 K but its minimum 37-GHz PCT is 262. This is another artifact of a hot desert background. This storm actually does have substantial 37-GHz scattering - it is an intense summer storm in the Australian Outback. Emission by the hot surface produces a background 37-GHz PCT in excess of 330 K. Its larger footprint causes the 37-GHz channel to be more influenced by the surface emission.

Whether categorizing the precipitation features by minimum 85- or 37-GHz PCT, just over half the total rainfall comes from CAT-0 features (Table 2b,c). Almost 30% of the rain and ~3/4 of the lightning comes from the 1% of storms with the greatest ice scattering. Intense 37-GHz scattering is somewhat more closely related to flash production than is intense 85-GHz scattering: 35% of the flashes are produced by the top 0.1% (CAT-3-5) of features ranked by 37-GHz PCT, while 30% are produced by the top 0.1% ranked by 85-GHz PCT. For either ranking, this top 0.1% yields ~5% of all rainfall.

c. Categorization by size

Flash rate and minimum brightness temperature relate to a system's convective intensity. The characteristic reflectivity profiles in the previous stratifications demonstrate this. Precipitation feature size, on the other hand, is mostly independent of convective intensity. The reflectivity profiles do not distinguish one size category from another (Fig. 19). The median profile for the smallest (CAT-0) features is shallow and has low reflectivity. The median profiles for all other size categories are quite similar to each other, with reflectivity around 50 dBZ near the surface, decreasing to around 30 dBZ at -15° C, and 20 dBZ at -40° C. Likewise, the brightness temperatures only distinguish the smallest (CAT-0) features from the rest in Table 2e. The

median brightness temperatures are all around 200 K at 85-GHz and 260 K at 37-GHz for CAT-1-5 as determined by size. The median flash rate is 0 for all size classes. Most precipitation features, regardless of size, do not have detectable flash rates. While the smallest features (CAT-0) tend to be shallow and weak, all sizes are capable of producing deep, intense convection.

Precipitation feature size is somewhat more related to volumetric rain than are the indicators of convective intensity. Only ~1/3 of the total rainfall is produced by the smallest (CAT-0) features (Table 2e). This compares to 50-70% when the features are categorized by flash rate or brightness temperature instead of size. The largest 1% of all precipitation features produce half of the rainfall in the TRMM domain. They produce 1/3 of the lightning.

d. Categorization by volumetric rain

Like precipitation feature flash rate, volumetric rain combines effects of intense small-scale convection and the areal extent of the precipitation feature. As a result, the median reflectivity profiles sorted by volumetric rain (Fig. 20) are distinguishable as separate profiles (unlike the profiles sorted by feature size). The profiles are not as distinct as those sorted by flash rate or brightness temperature. While the profiles for CAT-1-4 are separated by only a few dBZ each, the CAT-5 profile has much greater reflectivity - e.g., 41 dBZ at –40° C versus 29 dBZ for the CAT-4 profile. There is a similar trend in brightness temperatures and especially flash rates, with the CAT-5 rainmakers producing much lower median brightness temperatures and much greater median flash rates than CAT-4. Precipitation feature size exerts the greatest control on volumetric rain, but the rainiest (CAT-5) systems often combine quite intense convection and a large raining area (Fig. 21).

With the precipitation features sorted by volumetric rain, the rainiest 1% contribute just over

half of the total rainfall (Table 2f). Each category's contribution to total rainfall is similar whether the precipitation features are sorted by size (Table 2e) or by volumetric rain (Table 2f). The exception is CAT-5, which contributes a factor of four less to total rainfall when the features are sorted by size. This implies that the largest features do not have a tendency for greater localized rain rates, they simply have an extensive area of mostly light-moderate rain. Examination of individual cases confirms this.

Besides contributing half of the total TRMM rainfall, the rainiest 1% of features also contribute half of the lightning flashes. For all categories in Table 2f, the contribution to total rainfall is roughly similar to the contribution to total flash rate. The converse is not true - with features sorted by their flash rates (Table 2a), the contribution to total flash rate is not proportionate to the contribution to total rainfall.

5. Discussion and summary

A three-year sample of nearly six million precipitation features has been documented in terms of individual storm flash rate, convective intensity (minimum brightness temperature and vertical profile of maximum reflectivity), size, and volumetric rainfall. The population is dominated by the smallest storms, with no lightning and very weak radar and radiometric signatures. 97.6% do not have detected lightning, with the minimum detectable flash rate 0.7 fl min^{-1}. A crude land/ocean separation reveals that ~10% of precipitation features over land and ~1% of precipitation features over oceans have detected lightning (Fig. 1a). For a three-month subset of these precipitation features, Toracinta et al. (2002) found that 12-15% of precipitation features in Tropical South America and Tropical Africa and 0.2-0.3% of precipitation features in

the Tropical West Pacific and Tropical East Pacific had lightning. Besides the order of magnitude difference in thunderstorm occurrence, individual storm flash rates are at least a factor of two greater in the storms over land (Fig. 1c). That is, the very high flash rates occur even more often over land. The initial three-month study by Nesbitt et al. (2000) similarly found an order of magnitude difference in the frequency of thunderstorm occurrence for Tropical South America and Tropical Africa compared to the Tropical West Pacific and Tropical East Pacific, but found two orders of magnitude difference for thunderstorms having at least 10 flashes. Toracinta and Zipser (2001) found high flash rate storms (using the Optical Transient Detector) to be located almost exclusively over land. The estimates of the land/ocean differences are conservative in this paper, due to the crude land/ocean distinction. These will be more carefully analyzed in Part II of this paper. The precipitation features with no lightning or sub-detectable flash rates contribute 69% of the total rainfall.

The precipitation features have been ranked by flash rate, convective intensity, size, and volumetric rainfall. They have subsequently been assigned to categories emphasizing the rare but extremely large and/or vigorous events. The top 1% of precipitation features ranked by flash rate contribute 90% of the lightning and 21% of the rainfall. Almost half of the lightning is produced by storms with intermediate flash rates (2.2-31 fl min^{-1}), while 1/8 of all lightning comes from the top 0.01% of precipitation features, those having at least 122 fl min^{-1}. The storms with intermediate flash rates may deserve the most attention for issues involving the global electrical circuit or lightning's impact on atmospheric chemistry, but the rare storms with very high flash rates need to be properly sampled and treated.

Considering the storms' convective intensities as indicated by passive microwave ice

scattering at 85- and 37-GHz, the 1% of precipitation features with the greatest magnitude of ice scattering account for more than 1/4 of the rainfall and ~3/4 of the lightning in the TRMM domain. Nesbitt et al. (2000) found that the 1.5% of precipitation features qualifying as mesoscale convective systems (according to size and 85 GHz scattering thresholds) contribute roughly half of the total rainfall and lightning. Using 85 GHz alone to identify precipitation systems and their rainrates, Mohr et al. (1999) found the MCS population to contribute ~3/4 of the rainfall. They found that the largest 1% of their systems contribute ~1/3 of the rainfall. A fundamental difference between this study and that by Mohr et al. is the ability to identify rain without a significant 85 GHz ice scattering signature, thanks to the use of the Precipitation Radar. The size of the raining area is much more closely related to total volumetric rainfall than to lightning production. The largest 1% of precipitation features account for half of the rainfall but only 1/3 of the lightning in this study. Thus for precipitation estimation, it is most important to accurately discriminate between raining and non-raining pixels.

The most extreme storms according to one property are also superlative according to the other properties. The main exception to this is that total precipitation feature area has little to do with convective intensity. Precipitation features with the *greatest flash rates* necessarily include intense (CAT-3 or greater) convection as revealed by their passive microwave ice scattering and radar reflectivity profiles. The highest flash rate storms are also all large systems, likely containing several strong convective cells. These extreme flash rates do not result from merely having a large collection of ordinary thunderstorms. The *largest precipitation features*, on the other hand, tend to be extensive rain areas over the oceans without particularly intense convection. Most are associated with extratropical cyclones. These are deep, glaciated systems,

but most do not have lightning. These extremely large precipitation features are prolific rainmakers. The *most extreme volumetric rain* storms are all large precipitation features, and most do include intense convection. The combination of precipitation feature size and convective intensity often leads to very high flash rates, although in some cases a lack of convective intensity is countered by an extreme horizontal extent.

The simultaneous measurement of lightning flash rate, passive microwave brightness temperature, and radar reflectivity profiles allows quantification of the probability that a storm will produce lightning, given its brightness temperature or radar reflectivity. Roughly 1/4 of precipitation features having 200 K minimum 85-GHz PCT produce lightning (as detected by LIS). Almost half of the features producing lower 85-GHz PCT also produce lightning. Such probabilities for any particular brightness temperature threshold are presented in Fig. 3c, 4c. For a given brightness temperature, there is a much greater likelihood of lightning in continental storms than in oceanic storms. The continental-versus-oceanic contrast is even greater in Fig. 1-2 of Cecil and Zipser (2002), which uses a smaller (3 month) sample but more carefully distinguishes between continental and oceanic regions. These probabilities can be applied to gauging the aviation hazard from individual storms, or inferring pseudo-climatologies of lightning from long-term brightness temperature records.

The probability of lightning occurrence as a function of radar reflectivity and temperature (height) (Fig. 8e-f) agrees with thresholds for storm electrification identified in previous studies. The database in this study allows much greater interpretation of such thresholds in probabilistic terms. For example, 40 dBZ at $-10°$ C is a precursor for lightning identified by several investigators (Dye et al. 1989; Buechler and Goodman 1990; Gremillion and Orville 1999). The

TRMM database reveals that half of all precipitation features reaching this threshold also have lightning detected by LIS. With 40 dBZ extending further into the mixed phase region, to –20° C, 90% of features have lightning. When the reflectivity at this -20° C level only reaches 30 dBZ, only one quarter of the precipitation features have LIS-detected lightning. These probabilities for any combination of reflectivity and temperature are presented in Fig. 8c. Again, there is a substantial land/ocean difference. For continental and oceanic storms having the same reflectivities, the continental storms are more likely to produce lightning.

The basic land/ocean contrast in accumulated lightning flash rates (Fig. 2; Brooks 1925; Orville and Henderson 1986; Boccippio et al. 2000; Christian et al. 2003; many others) results from at least two contributing land/ocean contrasts. Intense, deep convection (as inferred from radar and radiometer) occurs about an order of magnitude more frequently in continental environments than in oceanic environments (Fig. 3a, 4a, 8b; Mohr and Zipser 1996; Nesbitt et al. 2000; Petersen and Rutledge 2001; Toracinta et al. 2002; many others) despite roughly similar thermodynamic instability in continental and oceanic environments (Williams and Renno 1993; Lucas et al. 1996). Additionally, storms which appear to be equals in terms of their updraft velocities and ice mass (as inferred from ice scattering signatures and radar reflectivity profiles) are more likely to produce lightning when they occur in continental environments, compared to those occurring in oceanic environments (Fig. 3c, 4c, 8f; Toracinta et al. 2002, Cecil and Zipser 2002). An explanation for the land/ocean contrast in accumulated lightning flash rates must therefore allow for (1) more intense convection with greater updrafts and larger ice in continental regimes, even when thermodynamic instability is comparable in oceanic regimes and (2) more lightning from continental thunderstorms, even when compared to those oceanic storms which

otherwise appear to have similarly intense convection. There are likely multiple factors contributing to these observed land/ocean contrasts. Some of the possibilities are summarized below.

Continental environments tend to have deeper boundary layers and higher cloud bases due to greater surface sensible heat flux and lower relative humidity. This supports broader continental updrafts, and a greater depth of precipitation growth below the freezing level in oceanic clouds (Lucas et al. 1994; Williams and Stanfill 2002; Williams et al. 2004). Broader updrafts are less susceptible to entrainment, and therefore capable of realizing greater buoyancy. This favors more intense convection (greater updraft speeds) in continental regimes. The deep layer of warm precipitation growth by collision-coalescence in oceanic clouds results in depletion of small droplets and enhancement of rainout below the freezing level. This yields greater precipitation loading low in the cloud, and also reduces the contribution to buoyancy from the latent heat of fusion (Zipser and Lutz 1994; Zipser 2003) if greater water mass rains out of the cloud before freezing. Again, this favors more intense convection in continental regimes. The growth of large, precipitating raindrops below the freezing level in oceanic clouds also leaves less residual cloud water available to become supercooled. Supercooled liquid water is critical for the separation of charge during collisions between graupel or hail and cloud ice (Takahashi 1978; Saunders and Peck 1998; many others). Therefore, low cloud base heights would contribute to a decreased likelihood of lightning (due to decreased supercooled water) for a given convective intensity.

Differing aerosol concentrations have also been proposed as a factor in the observed land/ocean contrasts (Rosenfeld and Lensky 1998; Williams et al. 2002). An aerosol-rich continental environment allows the water mass to be distributed over many small droplets,

compared to a spectrum with larger drops in an aerosol-poor oceanic environment. Similar to the discussion above involving low oceanic cloud bases, this could contribute to greater updraft speeds in continental convection (from latent heat of fusion when small water droplets freeze during graupel growth or during homogeneous nucleation near -40 C). It could also contribute to less electrification (due to decreased supercooled water) in oceanic updrafts, even when proxies for convective intensity appear comparable to those in continental storms with greater electrification.

Surface inhomogeneities provide a ready source of mesoscale boundaries over many land regions. These boundaries organize mesoscale ascent, focusing convective growth in particular zones. This mesoscale forcing maximizes updraft size and minimizes the deleterious effects of entrainment. The reduced entrainment allows greater updraft speeds and more intense convection in such regimes.

Some or all of these processes, and possibly others, likely act in concert to yield the observed differences in convection and lightning for continental and oceanic regimes. It is important to note that continental-like convective regimes often exist over water and oceanic-like convective regimes often exist over land. Many locations vary in their convective character throughout the year. Ultimately, explanations for the land/ocean differences need to allow for this.

The results here composite the characteristics of precipitation features throughout the global tropics and subtropics during a three-year period. The results therefore have nearly global applicability, with the understanding that variability exists from region to region (e.g., Toracinta et al. 2002) and from meteorological regime to regime (e.g., Cecil et al. 2002). This is a topic of further study, which will be presented in PART II of this paper. The bulk composite presented

here provides a context for measurements made in particular regional / seasonal / or meteorological domains, or for particular case studies.

Acknowledgments:

Thanks to the TRMM Science Data and Information System (TSDIS) for providing data and Dr. Baike Xi for her role in data processing. Dr. Rob Cifelli and an anonymous reviewer provided valuable suggestions for this manuscript. This research has been sponsored by NASA.

REFERENCES:

Adler, R. F., H.-Y. M. Yeh, N. Prasad, W.-K. Tao, J. Simpson, 1991: Microwave simulations of a tropical rainfall system with a three-dimensional cloud model. *J. Appl. Meteor.*, **30**, 924-953.

Boccippio, D. J., S. J. Goodman, and S. Heckman, 2000: Regional differences in tropical lightning distributions. *J. Appl. Meteor.*, **39**, 2231-2248.

Boccippio, D. J., W. J. Koshak, R. J. Blakeslee, 2002: Performance assessment of the Optical Transient Detector and Lightning Imaging Sensor. Part I: Predicted diurnal variability. *J. Atmos. Oceanic Tech.*, **19**, 1318-1332.

Brooks, C. E. P., 1925: The distribution of thunderstorms over the globe, *Geophys. Mem. London*, **24**, 147-164.

Buechler, D. E. and S. J. Goodman, 1990: Echo size and asymmetry: Impact on NEXRAD storm identification. *J. Appl. Meteor.*, **29**, 962-969.

Carey, L. D. and S. A. Rutledge, 2000: The relationship between precipitation and lightning in tropical island convection: A C-band polarimetric radar study. *Mon. Wea. Rev.*, **128**, 2687-2710.

Cecil, D. J., E. J. Zipser, and S. W. Nesbitt, 2002: Reflectivity, ice scattering, and lightning characteristics of hurricane eyewalls and rainbands. Part I: Quantitative description. *Mon. Wea. Rev.*, **130**, 769-784.

Cecil, D. J. and E. J. Zipser, 2002: Reflectivity, ice scattering, and lightning characteristics of hurricane eyewalls and rainbands. Part II: Intercomparison of observations. *Mon. Wea. Rev.*,

130, 785-801.

Christian, H. J., R. J. Blakeslee, S. J. Goodman, D. A. Mach, M. F. Stewart, D. E. Buechler, W. J. Koshak, J. M. Hall, W. L. Boeck, K. T. Driscoll, and D. J. Boccippio, 1999: The Lightning Imaging Sensor. *Proc. 11th International Conf. On Atmospheric Electricity*, Guntersville, AL, International Commission on Atmospheric Electricity, 746-749. [Available from NASA Center for Aerospace Information, 800 Elkridge Landing Rd, Linthicum Heights, MD 21090-2934.]

Christian, H. J., R. J. Blakeslee, D. J. Boccippio, W. L. Boeck, D. E. Buechler, K. T. Driscoll, S. J. Goodman, J. M. Hall, W. J. Koshak, D. M. Mach, M. F. Stewart, 2003: Global frequency and distribution of lightning as observed from space by the Optical Transient Detector. *J. Geophys. Res.*, **108**(D1), 2347-2363.

Dye, J. E., W. P. Winn, J. J. Jones, and D. W. Breed, 1989: The electrification of New Mexico thunderstorms. Part I: The relationship between precipitation development and the onset of electrification. *J. Geophys. Res.*, **94**, 8643-8656.

Gremillion, M. S. and R. E. Orville, 1999. Thunderstorm characteristics of cloud-to-ground lightning at the Kennedy Space Center, Florida: A study of lightning signatures as indicated by the WSR-88D. *Wea. Forecasting*, **14**, 640-649.

Kozu, T., T. Kawanishi, H. Kuroiwa, M. Kojima, K. Oikawa, H. Kumagai, K. Okamoto, M. Okumura, H. Nakatsuka and K. Nishikawa, 2001: Development of precipitation radar onboard the tropical rainfall measuring mission satellite. *IEEE Geosci. Remote Sens.*, **39**, 102-116.

Kummerow, C., W. Barnes, T. Kozu, J. Shiue, and J. Simpson, 1998: The Tropical Rainfall Measuring Mission (TRMM) sensor package. *J. Atmos. Ocean. Tech.*, **15**, 809-817.

Kummerow, C., J. Simpson, O. Thiele, W. Barnes, A. T. C. Chang, E. Stocker, R. F. Adler, A. Hou, R. Kakar, F. Wentz, P. Ashcroft, T. Kozu, Y. Hong, K. Okamoto, T. Iguchi, H. Kuroiwa, E. Im, Z. Haddad, G. Huffman, B. Ferrier, W. S. Olson, E. Zipser, E. A. Smith, T. T. Wilheit, G. North, T. Krishnamurti, K. Nakamura, 2000: The status of the Tropical Rainfall Measuring Mission (TRMM) after two years in orbit. *J. Appl. Meteor.*, **39**, 1965-1982.

Lucas, C., E. J. Zipser, and M. A. LeMone, 1994: Vertical velocity in oceanic convection off tropical Australia. *J. Atmos. Sci.*, **51**, 3344-3350.

Lucas, C., E. J. Zipser, and M. A. LeMone, 1996: Reply. *J. Atmos. Sci.*, **53**, 1212-1216.

Marshall, J. S. and S. Radhakant, 1978: Radar precipitation maps as lightning indicators. *J. Appl. Meteor.*, **17**, 206-212.

McCollum, J. R. and R. R. Ferraro, 2003: Next generation of NOAA/NESDIS TMI, SSM/I, and AMSR-E microwave land rainfall algorithms. *J. Geophys. Res.*, **108**(d8), 8382-8398.

Michimoto, K., 1991: A study of radar echoes and their relation to lightning discharge of thunderclouds in the Hokuriku District. Part I: Observation and analysis of thunderclouds in summer and winter. *J. Meteor. Soc. Japan*, **69**, 327-335.

Mohr, K. I. and E. J. Zipser, 1996: Defining mesoscale convective systems by their 85-GHz ice-scattering signatures. *Bull. Amer. Meteor. Soc.*, **77**, 1179-1189.

Mohr, K. I., E. R. Toracinta, E. J. Zipser, and R. E. Orville, 1996: A comparison of WSR-88D

reflectivities, SSM/I brightness temperatures, and lightning for mesoscale convective systems in Texas. Part II: SSM/I brightness temperatures and lightning. *J. Appl. Meteor.*, **35**, 919-931.

Mohr, K. I., J. S. Famiglietti, and E. J. Zipser, 1999: The contribution to tropical rainfall with respect to convective system type, size, and intensity estimated from the 85-GHz ice-scattering signature. *J. Appl. Meteor.*, **38**, 596-605.

Nesbitt, S. W., E. J. Zipser, and D. J. Cecil, 2000: A census of precipitation features in the Tropics using TRMM: Radar, ice scattering, and lightning observations. *J. Climate*, **13**, 4087-4106.

Nesbitt, S. W. and E. J. Zipser, 2003: The diurnal cycle of rainfall and convective intensity according to three years of TRMM measurements. *J. Climate*, **16**, 1456-1475.

Orville, R. E. and R. W. Henderson, 1986: Global distribution of midnight lightning: September 1977 to August 1978. *Mon. Wea. Rev.*, **114**, 2640-2653.

Petersen, W. A. and S. A. Rutledge, 2001: Regional variability in tropical convection: Observations from TRMM. *J. Climate*, **14**, 3566-3586.

Rosenfeld, D. and I. M. Lensky, 1998: Satellite-based insights into precipitation formation processes in continental and maritime convective clouds. *Bull. Amer. Meteor. Soc.*, **79**, 2457-2476.

Saunders, C. P. R., and S. L. Peck, 1998: Laboratory studies of the influence of the rime accretion rate on charge transfer during crystal/graupel collisions. *J. Geophys. Res.*, **103** (D12), 13949-13956.

Shackford, C. R., 1960: Radar indications of precipitation-lightning relationships in New

England thunderstorms. *J. Atmos. Sci.*, **17**, 15-19.

Skofronick-Jackson, G. M. and J. R. Wang, 2000: The estimation of hydrometeor profiles from wideband microwave observations. *J. Appl. Meteor.*, **39**, 1645-1657.

Smith, E. A., A. Mugnai, H. J. Cooper, G. J. Tripoli, and X. Xiang, 1992: Foundations for statistical physical precipitation retrieval from passive microwave satellite measurements. Part I: Brightness temperature properties of a time-dependent cloud radiation model. *J. Appl. Meteor.*, **31**, 506-531.

Spencer, R. W., 1986: A satellite passive 37-GHz scattering-based method for measuring oceanic rain rates. *J. Appl. Meteor.*, **25**, 754-766.

Spencer, R. W., H. M. Goodman, and R. E. Hood, 1989: Precipitation retrieval over land and ocean with the SSM/I: Identification and characteristics of the scattering signal. *J. Atmos., Oceanic Tech.*, **6**, 254-273.

Takahashi, T., 1978: Riming electrification as a charge generation mechanism in thunderstorms. *J. Atmos. Sci.*, **35**, 1536-1548.

Toracinta, E. R., K. I. Mohr, E. J. Zipser, and R. E. Orville, 1996: A comparison of WSR-88D reflectivities, SSM/I brightness temperatures, and lightning for mesoscale convective systems in Texas. Part I: Radar reflectivity and lightning. *J. Appl. Meteor.*, **35**, 902-918.

Toracinta, E. R. and E. J. Zipser, 2001: Lightning and SSM/I-ice-scattering mesoscale convective systems in the global tropics. *J. Appl. Meteor.*, **40**, 983-1002.

Toracinta, E. R., D. J. Cecil, E. J. Zipser, and S. W. Nesbitt, 2002: Radar, passive microwave, and lightning characteristics of precipitating systems in the Tropics. *Mon. Wea. Rev.*, **130**,

802-824.

Vivekanandan, J., J. Turk, G. L. Stephens, and V. N. Bringi, 1990: Microwave radiative transfer studies using combined multiparameter radar and radiometer measurements during COHMEX. *J. Appl. Meteor.*, **29**, 561-585.

Vivekanandan, J., J. Turk, and V. N. Bringi, 1991: Ice water path estimation and characterization using passive microwave radiometry. *J. Appl. Meteor.*, **30**, 1407-1421.

Williams, E. R. and N. O. Renno, 1993: An analysis of the conditional instability in the tropical atmosphere. *Mon. Wea. Rev.*, **121**, 21-36.

Williams, E. R. and S. Stanfill, 2002: The physical origin of the land-ocean contrast in lightning activity. *Appl. Phys.*, **3**, 1277-1292.

Williams, E. R. and co-authors, 2002: Contrasting convective regimes over the Amazon: Implications for cloud electrification. *J. Geophys. Res.*, **107**(D20), 380-398.

Williams, E. R., V. Mushtak, D. Rosenfeld, S. Goodman, and D. Boccippio, 2004: Thermodynamic conditions favorable to superlative thunderstorm updraft, mixed phase microphysics and lightning flash rate. Submitted to *Atmos. Res.*

Zipser, E. J. and K. R. Lutz, 1994: The vertical profile of radar reflectivity of convective cells: A strong indicator of storm intensity and lightning probability? *Mon. Wea. Rev.*, **122**, 1751-1759.

Zipser, E. J., 2003: Some views on 'hot towers" after 50 years of tropical field programs and two years of TRMM data. *Meteor. Mono.*, **51**, 49-58.

TABLE CAPTIONS

Table 1. Range of values defining each Precipitation Feature category.

Table 2. (a) Minimum, median, and maximum value of each Precipitation Feature property for each ***flash rate*** category.

Table 2. (b) Minimum, median, and maximum value of each Precipitation Feature property for each ***minimum 85-GHz PCT*** category.

Table 2. (c) Minimum, median, and maximum value of each Precipitation Feature property for each ***minimum 37-GHz PCT*** category.

Table 2. (d) Minimum, median, and maximum value of each Precipitation Feature property for each ***area with 85-GHz ≤150 K*** category. Categories 0-2 are undefined.

Table 2. (e) Minimum, median, and maximum value of each Precipitation Feature property for each ***total area*** category.

Table 2. (f) Minimum, median, and maximum value of each Precipitation Feature property for each ***volumetric rain*** category.

FIGURE CAPTIONS

Figure 1. (a) Probability (thin) and Cumulative (thick) Density Functions of precipitation feature flash rate (uncorrected for detection efficiency). (b) Extrapolation of Cumulative Density Function to very low flash rates. (c) Flash rate distributions among precipitation features *with detected lightning* only. Land = dashed line; water = dotted line; total = solid line.

Figure 2. Precipitation features with LIS-observed lightning as a function of flash rate category (CAT-1-5).

Figure 3. (a) Probability (thin) and Cumulative (thick) Density Functions of minimum 85-GHz PCT. (b) Precipitation features *with detected lightning* only. (c) Probability that a precipitation feature has lightning, given its minimum 85-GHz PCT. Land = dashed line; water = dotted line; total = solid line.

Figure 4. (a) Probability (thin) and Cumulative (thick) Density Functions of minimum 37-GHz PCT. (b) Precipitation features *with detected lightning* only. (c) Probability that a precipitation feature has lightning, given its minimum 37-GHz PCT. Land = dashed line; water = dotted line; total = solid line.

Figure 5. (a) Probability (thin) and Cumulative (thick) Density Functions of precipitation feature size (km^2). (b) Precipitation features *with detected lightning* only. (c) Probability that a precipitation feature has lightning, given its size. Land = dashed line; water = dotted line; total = solid line.

Figure 6. (a) Probability (thin) and Cumulative (thick) Density Functions of areal extent of strong convection (85-GHz < 150 K) (km^2). (b) Precipitation features *with detected lightning*

only. (c) Probability that a precipitation feature has lightning, given its areal extent of strong convection. Land = dashed line; water = dotted line; total = solid line.

Figure 7. (a) Probability (thin) and Cumulative (thick) Density Functions of volumetric rain (mm km^2 h^{-1}). (b) Precipitation features *with detected lightning* only. (c) Probability that a precipitation feature has lightning, given its volumetric rain. Land = dashed line; water = dotted line; total = solid line.

Figure 8. Cumulative Density Functions of maximum radar reflectivity (dBZ), with environmental temperature as the vertical coordinate. (a) all precipitation features; (b) precipitation features over land (dashed) and water (solid); median and 99.9th percentile in bold; (c) precipitation features *with detected lightning*; (d) precipitation features with detected lightning over land (dashed) and water (solid); median and 99.9th percentile in bold; (e) probability that a precipitation feature has lightning, given its maximum reflectivity; (f) probability that a precipitation feature over land (dashed) or water (solid) has lightning, given its maximum reflectivity.

Figure 9. Vertical profiles of minimum (small italic numerals, dotted lines), median (large bold numerals, solid lines), and maximum (bold italic numerals, dashed lines) precipitation feature maximum reflectivity for classes of precipitation features stratified by flash rate (CAT-0 - CAT-5) as in Table 1a. Near surface reflectivity is plotted at 10° C for convenience.

Figure 10. Scatterplot of precipitation feature minimum 37-GHz PCT versus areal extent of strong convection. Colors and symbols as in Fig. 2, corresponding to flash rate categories one through five (see Table 1a). Solid lines are contours of the frequency distribution, with 5 K and

100 km2 bin sizes and contours at 10^0, 10^1, 10^2, 10^3, 10^4, 10^5, 10^6 precipitation features. Blue line is the median areal extent of strong convection for each 37-GHz PCT value.

Figure 11. (a) 85-GHz PCT for precipitation feature over India, 26 Aug 2000. Dashed black line marks edge of PR swath. The precipitation feature of interest is marked with black dots. Lightning flash locations marked with black symbols. (b) Vertical cross-section of reflectivity along the dashed white line in (a). Black lines are 85-GHz PCT (solid) and 37-GHz PCT (dashed) nearest the cross section.

Figure 12. As in Fig. 11 (different horizontal scale), for precipitation feature near Argentina-Paraguay border, 17 Nov 1998. Lightning flash locations omitted for legibility.

Figure 13. As in Fig. 11 (different horizontal scale), for precipitation feature over South Pacific, 21 Dec 1998. No lightning was detected.

Figure 14. As in Fig. 11 (different horizontal scale), for precipitation feature over West Africa, 26 May 2000.

Figure 15. As in Fig. 9, but stratified by minimum 85-GHz PCT.

Figure 16. As in Fig. 10, but with minimum 85-GHz PCT versus minimum 37-GHz PCT. Blue line is the median 37-GHz PCT for each 85-GHz PCT value.

Figure 17. As in Fig. 11 (different horizontal scale), for precipitation feature west of Brisbane, Australia, 27 Oct 1999. Lightning flash locations omitted for legibility.

Figure 18. As in Fig. 9, but stratified by minimum 37-GHz PCT.

Figure 19. As in Fig. 9, but stratified by size.

Figure 20. As in Fig. 9, but stratified by volumetric rain.

Figure 21. As in Fig. 10, but with minimum 37-GHz PCT versus size. Symbols correspond to volumetric rain categories one through five.

	Number	%	Flash Rate (Fl min^{-1})	Min 85-GHz (K)	Min 37-GHz (K)	Area ≤150 K (km^2)	Total Area (km^2)	Vol. Rain (mm h^{-1} km^2)
CAT-0	5,592,052	97.6	0-0	≥ 191	≥ 260	undefined	≤ 3940	0-14100
CAT-1	77,668	1.4	0.7-2.2	190-160	260-253	undefined	3941-10915	14100-41110
CAT-2	51,543	0.9	2.2-30.9	160-106	253-219	undefined	10915-51837	41110-228100
CAT-3	5154	0.09	30.9-122	105-74	219-177	425-1572	51837-111444	228200-528100
CAT-4	515	0.009	122-296	74-57	177-135	1573-3811	111518-186868	528600-942700
CAT-5	58	0.001	≥ 297	≤ 56	≤ 134	≥ 3866	≥187016	≥ 946200

Table 1. Range of values defining each Precipitation Feature category.

	CAT-0	*CAT-1*	*CAT-2*	*CAT-3*	*CAT-4*	*CAT-5*
Flash Rate	**0**	**0.7**	**2.2**	**31**	**122**	**297**
(Flashes / minute)	**0**	**0.7**	**5.8**	**47**	**162**	**376**
	0	**2.2**	**31**	**122**	**295**	**1351**
% of total flash rate	0	9.8	46.9	30.7	9.8	2.8
Min 85-GHz	63	67	48	46	42	46
(K)	278	207	162	110	84	71
	319	312	306	225	183	109
Min 37-GHz	193	187	109	110	69	99
(K)	281	267	253	217	181	151
	353	348	327	277	239	202
Area 85-GHz ≤150 K	0	0	0	0	0	0.6
(1000 km^2)	0	0	0	0.4	1.4	3.7
	1.8	3.1	2.9	5.5	8.1	20.1
Total Area	0.1	0.1	0.1	0.2	1.2	8.9
(1000 km^2)	0.1	0.8	2.1	7.6	18.8	40.2
	335	210.2	330.7	218.5	308.1	214.9
Volumetric Rain	0	0	0	1.2	19.3	128
(1000 mm km^2 h^{-1})	0.3	4.6	15.0	66.5	180	438
	1273	897	1701	1354	1608	2018
% of total volumetric rain	68.8	10	15.3	4.5	1.1	0.3

Table 2a. Minimum, median, and maximum value of each Precipitation Feature property for each ***flash rate*** category.

	CAT-0	*CAT-1*	*CAT-2*	*CAT-3*	*CAT-4*	*CAT-5*
Flash Rate	0	0	0	0	0	7.2
(Flashes / minute)	0	0	2.2	25.1	79.5	162
	75	146	326	993	956	1351
% of total flash rate	14	14.5	41.4	22.8	6	1.3
Min 85-GHz	**191**	**160**	**106**	**74**	**57**	**42**
(K)	**278**	**178**	**143**	**96**	**69**	**53**
	319	**191**	**160**	**106**	**74**	**57**
Min 37-GHz	211	197	146	113	107	69
(K)	281	262	249	214	178	144
	353	299	284	262	233	192
Area 85-GHz ≤150 K	0	0	0	0.1	0.1	0.3
(1000 km^2)	0	0	0.1	0.5	1.3	2.3
	0	0	2.5	9.3	8.1	20.1
Total Area	0.1	0.1	0.1	0.2	0.5	0.9
(1000 km^2)	0.1	2.3	4.5	7.8	10.7	15.4
	335.4	330.7	308.1	173.4	214.9	127.3
Volumetric Rain	0	0	0	1.4	5.2	14.6
(1000 mm km^2 h^{-1})	0.3	11.0	26.2	57.2	90.0	153
	1273	1701	1534	2018	1778	1344
% of total volumetric rain	53.6	17.8	23.6	4.2	0.6	0.1

Table 2b. Minimum, median, and maximum value of each Precipitation Feature property for each ***minimum 85-GHz PCT*** category.

	CAT-0	*CAT-1*	*CAT-2*	*CAT-3*	*CAT-4*	*CAT-5*
Flash Rate	0	0	0	0	2.9	29
(Flashes / minute)	0	0	2.9	34	107	195
	51	107	291	576	993	1351
% of total flash rate	15.1	9.1	40.5	26.2	7.6	1.5
Min 85-GHz	105	102	65	48	48	42
(K)	278	203	148	100	75	63
	319	278	274	217	150	82
Min 37-GHz	**260**	**253**	**219**	**177**	**135**	**69**
(K)	**281**	**258**	**247**	**208**	**166**	**124**
	353	**260**	**253**	**219**	**177**	**135**
Area 85-GHz ≤150 K	0	0	0	0	0	0.4
(1000 km^2)	0	0	0.1	0.5	1.3	2.5
	0.2	0.4	2.1	6.7	10.2	20.1
Total Area	0.1	0.1	0.1	0.2	0.7	1.6
(1000 km^2)	0.1	1.4	3.7	7.7	12.9	16.1
	300	335	331	308	215	127
Volumetric Rain	0	0	0	0	6.8	10.9
(1000 mm km^2 h^{-1})	0.3	7.6	23.9	63.9	129	181
	739	1273	1701	2018	1778	1344
% of total volumetric rain	52.5	19	22.9	4.7	0.8	0.1

Table 2c. Minimum, median, and maximum value of each Precipitation Feature property for each ***minimum 37-GHz PCT*** category.

	CAT-3	*CAT-4*	*CAT-5*
Flash Rate	0	0	66
(Flashes / minute)	25	113	289
	530	504	1351
% of total flash rate	21.5	7.3	2.2
Min 85-GHz	48	46	42
(K)	103	79	68
	143	118	97
Min 37-GHz	109	99	69
(K)	216	183	150
	253	235	197
Area 85-GHz ≤150 K	**0.4**	**1.6**	**3.9**
(1000 km^2)	**0.6**	**2.1**	**5.3**
	1.6	**3.8**	**20.1**
Total Area	0.9	4.5	12.1
(1000 km^2)	13.8	26.4	48.1
	219	173	215
Volumetric Rain	6.1	21.3	153
(1000 mm km^2 h^{-1})	99.4	224	572
	1530	1978	2018
% of total volumetric rain	5.7	1.2	0.3

Table 2d. Minimum, median, and maximum value of each Precipitation Feature property for each ***area with 85-GHz ≤150 K*** category. Categories 0-2 are undefined.

	CAT-0	*CAT-1*	*CAT-2*	*CAT-3*	*CAT-4*	*CAT-5*
Flash Rate	0	0	0	0	0	0
(Flashes / minute)	0	0	0	0	0	0
	224	359	993	956	1351	560
% of total flash rate	43.8	23	28.4	4.2	0.6	0.1
Min 85-GHz	52	46	42	46	53	68
(K)	278	208	186	192	209	218
	319	279	273	259	249	249
Min 37-GHz	124	99	69	107	126	145
(K)	281	264	260	258	259	259
	353	284	279	271	269	264
Area 85-GHz ≤150 K	0	0	0	0	0	0
(1000 km^2)	0	0	0	0	0	0
	1.5	3.6	9.3	10.2	20.1	8.0
Total Area	**0.1**	**3.9**	**10.9**	**51.9**	**112**	**187**
(1000 km^2)	**0.1**	**6.0**	**19.2**	**65.7**	**131**	**216**
	3.9	**10.9**	**51.9**	**112**	**187**	**335**
Volumetric Rain	0	1.3	5.4	39.8	128	285
(1000 mm km^2 h^{-1})	0.3	20.1	73.1	253	447	645
	111	255	1213	1978	2018	1778
% of total volumetric rain	34.9	14.6	36.8	11.3	2	0.3

Table 2e. Minimum, median, and maximum value of each Precipitation Feature property for each ***total area*** category.

	CAT-0	*CAT-1*	*CAT-2*	*CAT-3*	*CAT-4*	*CAT-5*
Flash Rate	0	0	0	0	0	0
(Flashes / minute)	0	0	0	0	3.6	121
	116	217	488	570	605	1351
% of total flash rate	26.3	23.9	36.9	9.2	2.5	0.6
Min 85-GHz	63	52	45	42	56	46
(K)	278	194	174	155	137	115
	319	289	274	249	239	221
Min 37-GHz	132	124	69	106	113	107
(K)	281	262	257	250	240	202
	353	292	278	266	263	260
Area 85-GHz ≤150 K	0	0	0	0	0	0
(1000 km^2)	0	0	0	0	0.1	1.0
	1.1	3.0	5.3	7.5	8.1	20.1
Total Area	0.1	0.1	0.3	10.1	26.7	50.2
(1000 km^2)	0.1	5.6	18.5	56.3	94.1	134
	31.4	64.5	149	286	308	335
Volumetric Rain	**0**	**14.1**	**41.1**	**229**	**529**	**953**
(1000 mm km^2 h^{-1})	**0.3**	**21.9**	**75.6**	**297**	**629**	**1191**
	14.1	**41.1**	**228**	**529**	**946**	**2018**
% of total volumetric rain	33.1	14.3	36.6	12.8	2.6	1.3

Table 2f. Minimum, median, and maximum value of each Precipitation Feature property for each ***volumetric rain*** category.

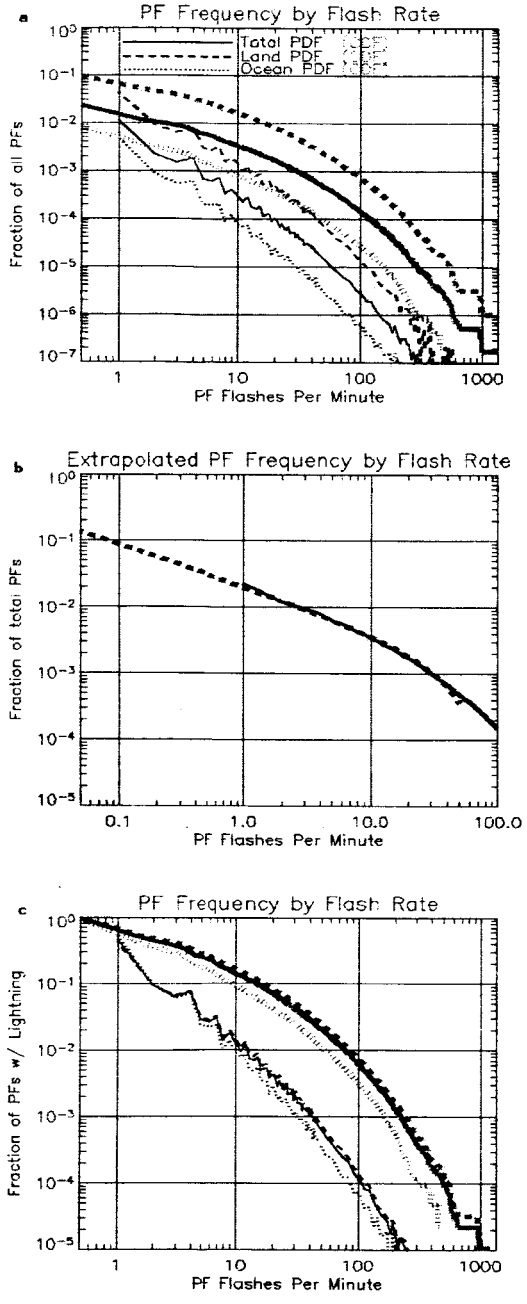

Fig. 1. (a) Probability (thin) and Cumulative (thick) Density Functions of precipitation feature flash rate (uncorrected for detection efficiency). (b) Extrapolation of Cumulative Density Function to very low flash rates. (c) Flash rate distributions among precipitation features *with detected lightning* only. Land = dashed line; water = dotted line; total = solid line.

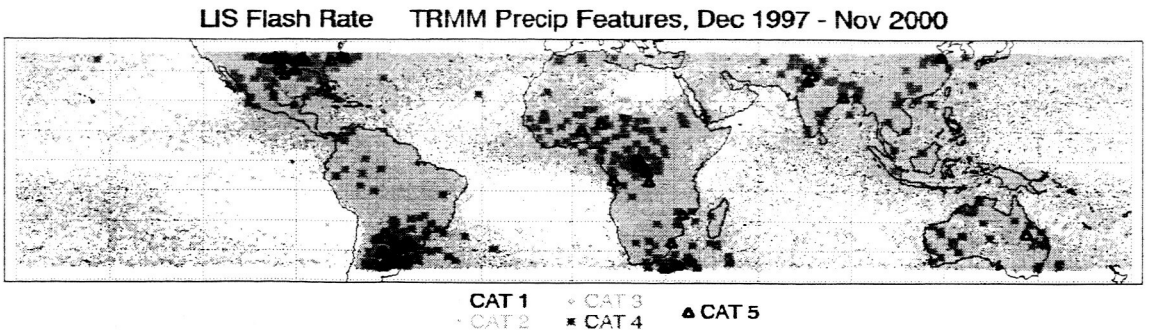

Fig. 2. Precipitation features with LIS-observed lightning as a function of flash rate category (CAT-1-5).

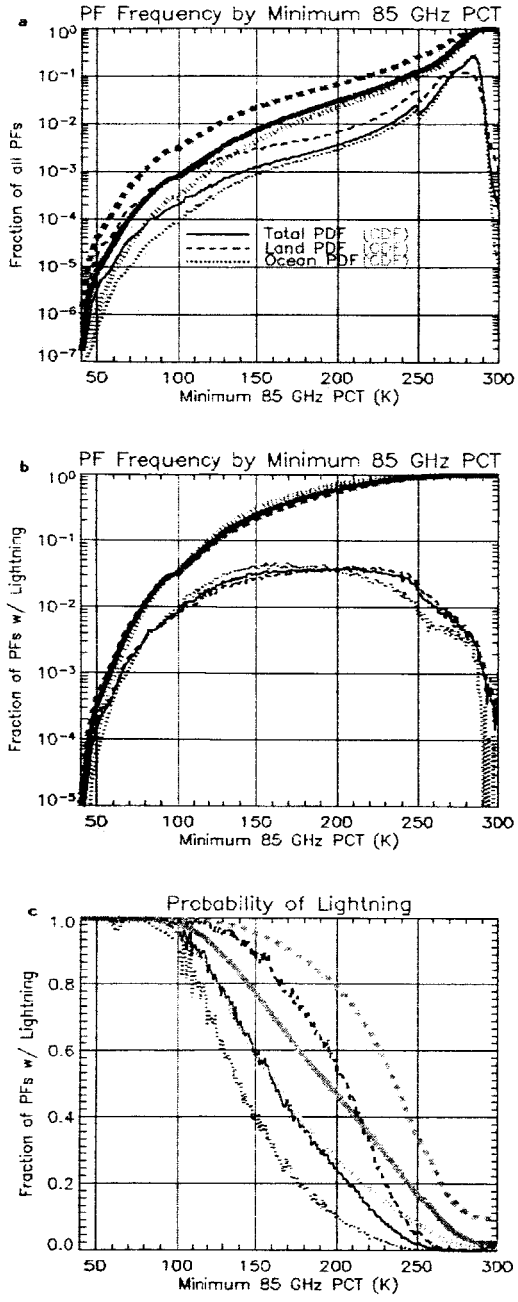

Fig. 3. (a) Probability (thin) and Cumulative (thick) Density Functions of minimum 85-GHz PCT. (b) Precipitation features *with detected lightning* only. (c) Probability that a precipitation feature has lightning, given its minimum 85-GHz PCT. Land = dashed line; water = dotted line; total = solid line.

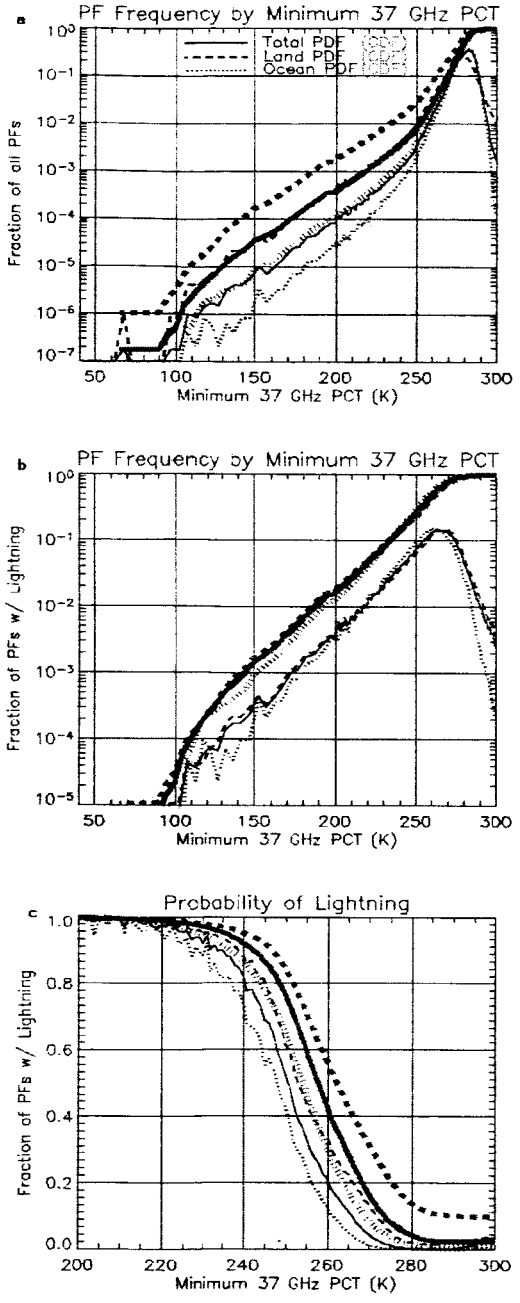

Fig. 4. (a) Probability (thin) and Cumulative (thick) Density Functions of minimum 37-GHz PCT. (b) Precipitation features *with detected lightning* only. (c) Probability that a precipitation feature has lightning, given its minimum 37-GHz PCT. Land = dashed line; water = dotted line; total = solid line.

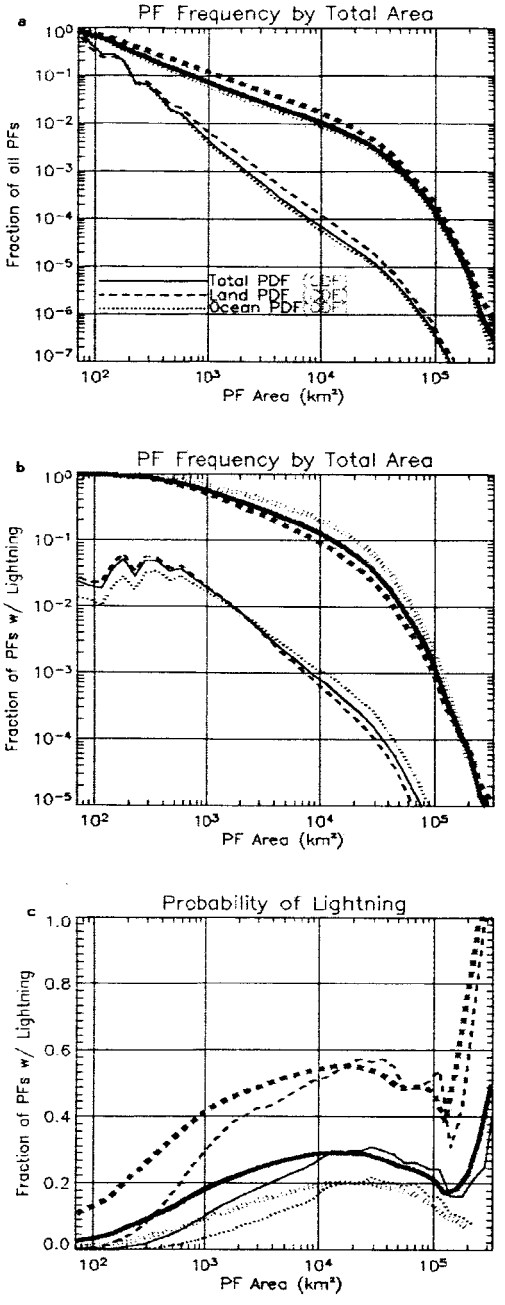

Fig. 5. (a) Probability (thin) and Cumulative (thick) Density Functions of precipitation feature size (km^2). (b) Precipitation features *with detected lightning* only. (c) Probability that a precipitation feature has lightning, given its size. Land = dashed line; water = dotted line; total = solid line.

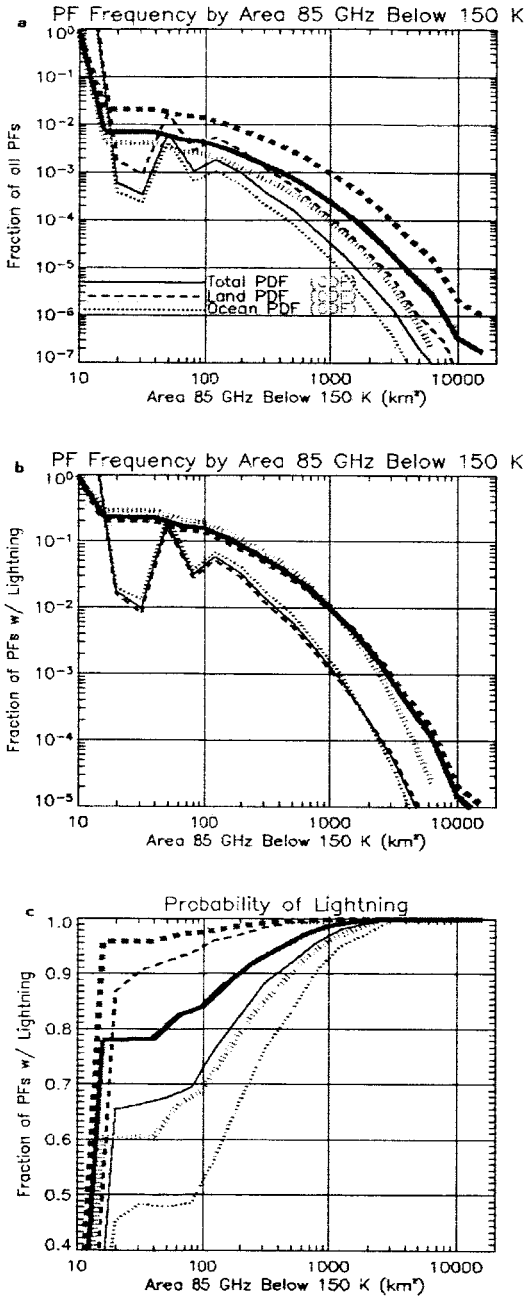

Fig. 6. (a) Probability (thin) and Cumulative (thick) Density Functions of areal extent of strong convection (85-GHz < 150 K) (km^2). (b) Precipitation features *with detected lightning* only. (c) Probability that a precipitation feature has lightning, given its areal extent of strong convection. Land = dashed line; water = dotted line; total = solid line.

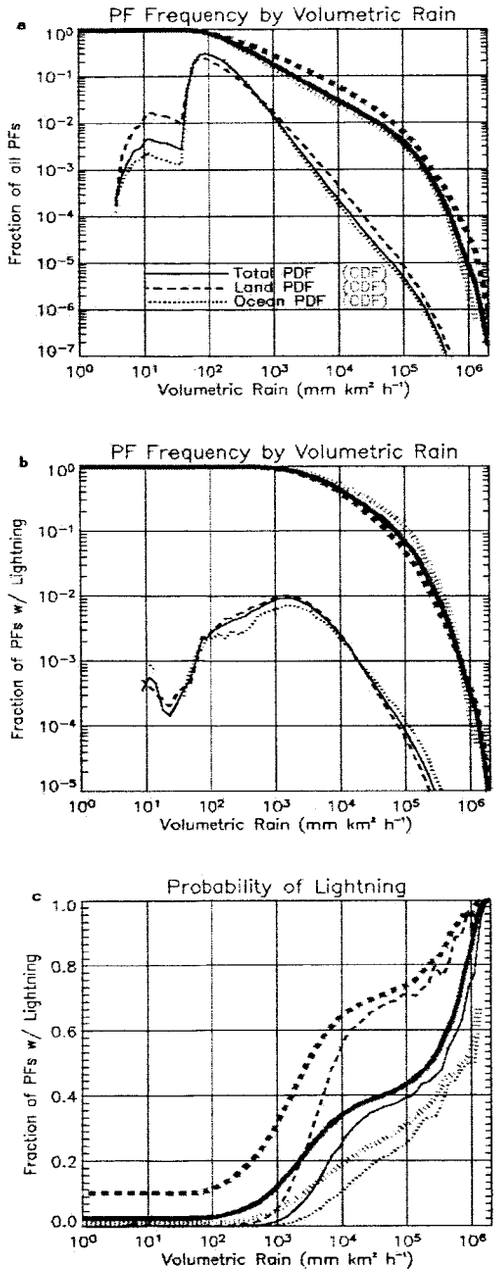

Fig. 7. (a) Probability (thin) and Cumulative (thick) Density Functions of volumetric rain (mm km^2 h^{-1}). (b) Precipitation features *with detected lightning* only. (c) Probability that a precipitation feature has lightning, given its volumetric rain. Land = dashed line; water = dotted line; total = solid line.

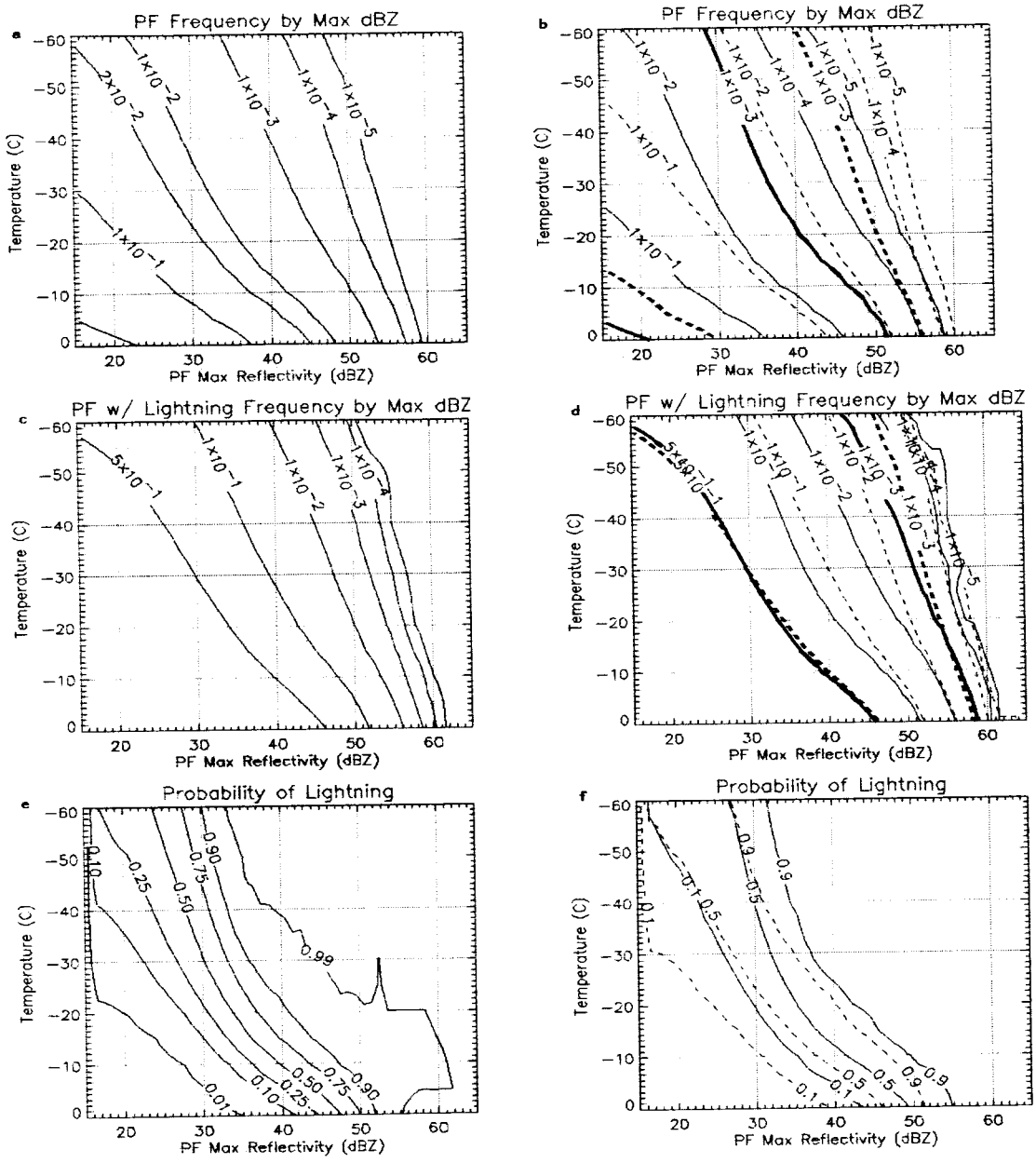

Fig. 8. Cumulative Density Functions of maximum radar reflectivity (dBZ), with environmental temperature as the vertical coordinate. (a) all precipitation features; (b) precipitation features over land (dashed) and water (solid); median and 99.9th percentile in bold; (c) precipitation features

with detected lightning; (d) precipitation features with detected lightning over land (dashed) and water (solid); median and 99.9th percentile in bold; (e) probability that a precipitation feature has lightning, given its maximum reflectivity; (f) probability that a precipitation feature over land (dashed) or water (solid) has lightning, given its maximum reflectivity.

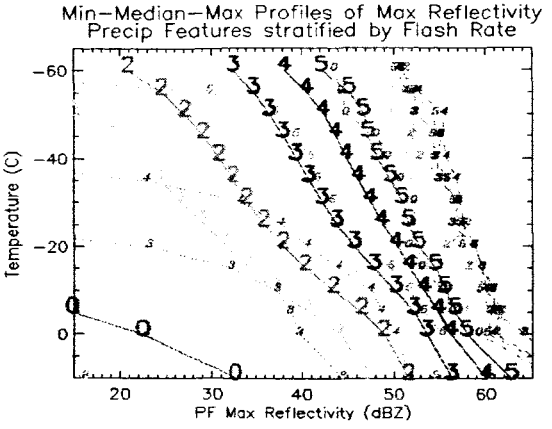

Fig. 9. Vertical profiles of minimum (small italic numerals, dotted lines), median (large bold numerals, solid lines), and maximum (bold italic numerals, dashed lines) precipitation feature maximum reflectivity for classes of precipitation features stratified by flash rate (CAT-0 - CAT-5) as in Table 1a. Near surface reflectivity is plotted at 10° C for convenience.

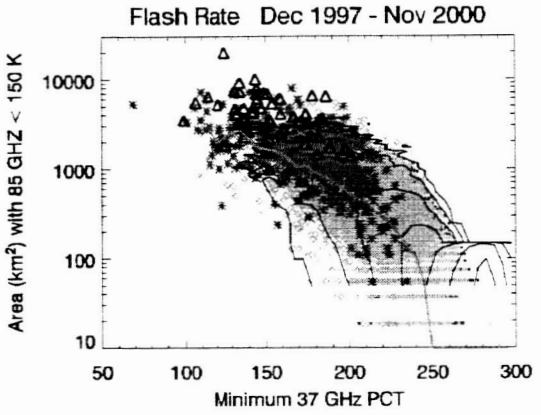

Fig. 10. Scatterplot of precipitation feature minimum 37-GHz PCT versus areal extent of strong convection. Colors and symbols as in Fig. 2, corresponding to flash rate categories one through five (see Table 1a). Solid lines are contours of the frequency distribution, with 5 K and 100 km2 bin sizes and contours at 10^0, 10^1, 10^2, 10^3, 10^4, 10^5, 10^6 precipitation features. Blue line is the median areal extent of strong convection for each 37-GHz PCT value.

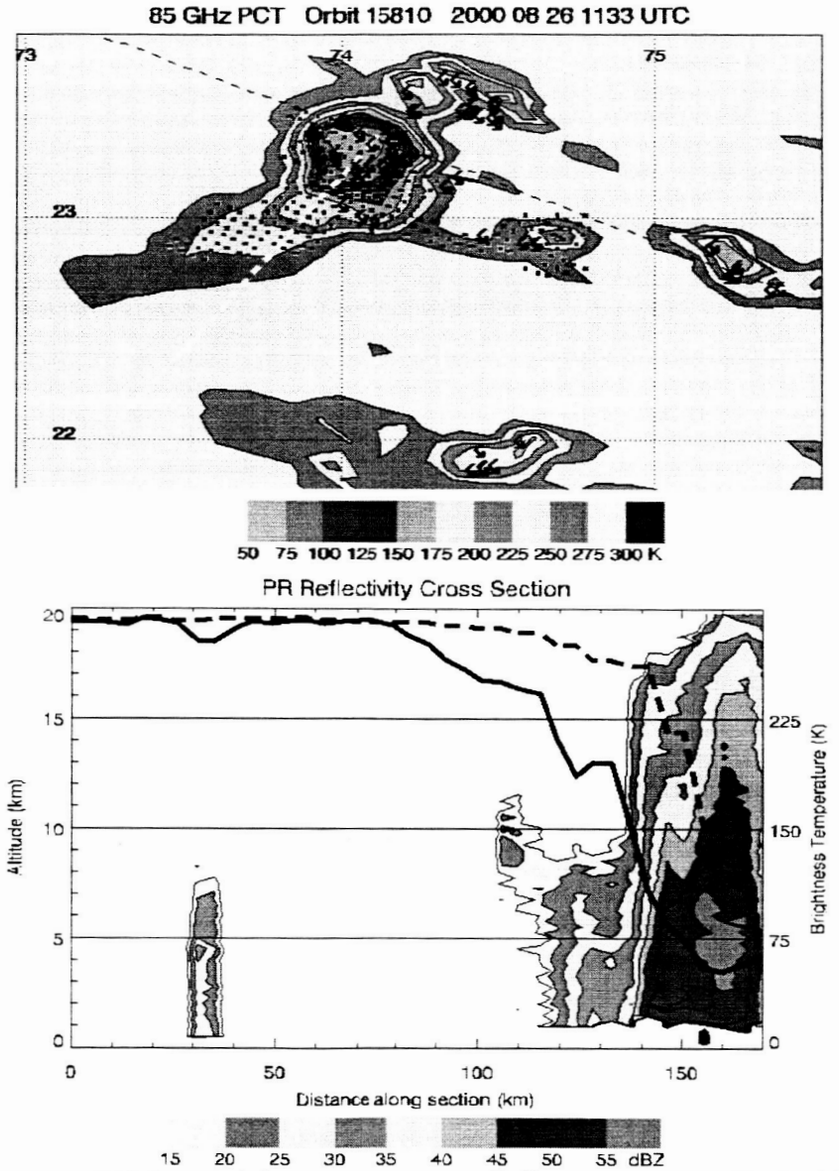

Fig. 11. (a) 85-GHz PCT for precipitation feature over India, 26 Aug 2000. Dashed black line marks edge of PR swath. The precipitation feature of interest is marked with black dots. Lightning flash locations marked with black symbols. (b) Vertical cross-section of reflectivity along the dashed white line in (a). Black lines are 85-GHz PCT (solid) and 37-GHz PCT (dashed) nearest the cross section.

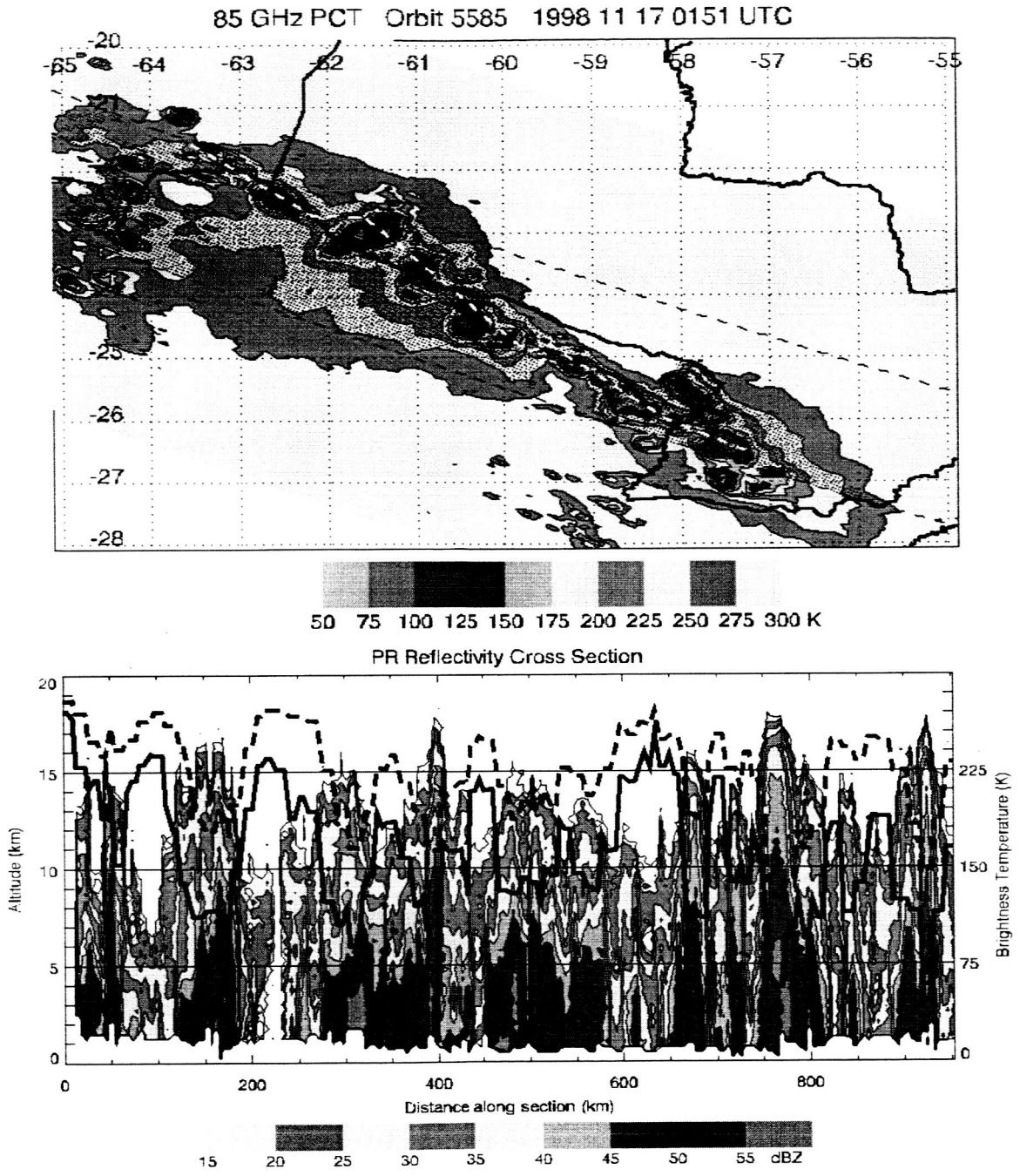

Fig. 12. As in Fig. 11 (different horizontal scale), for precipitation feature near Argentina-Paraguay border, 17 Nov 1998. Lightning flash locations omitted for legibility.

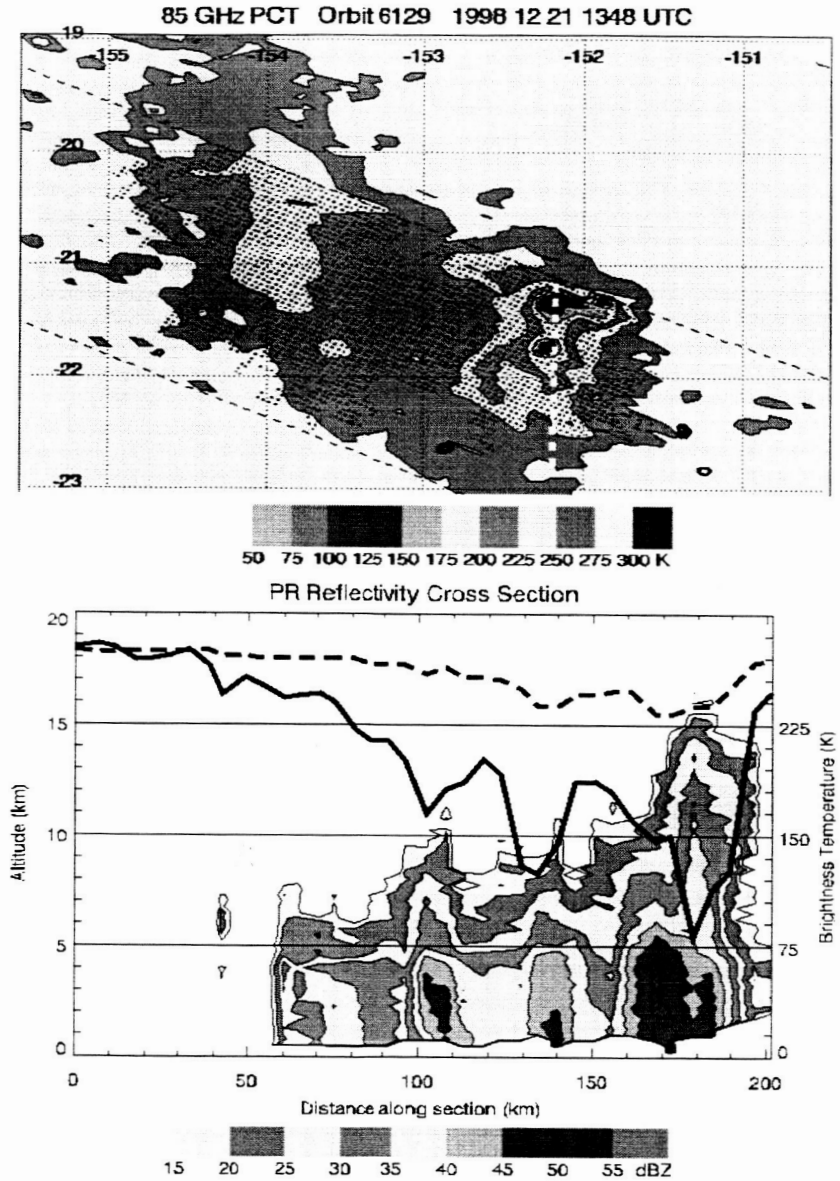

Fig. 13. As in Fig. 11 (different horizontal scale), for precipitation feature over South Pacific, 21 Dec 1998. No lightning was detected.

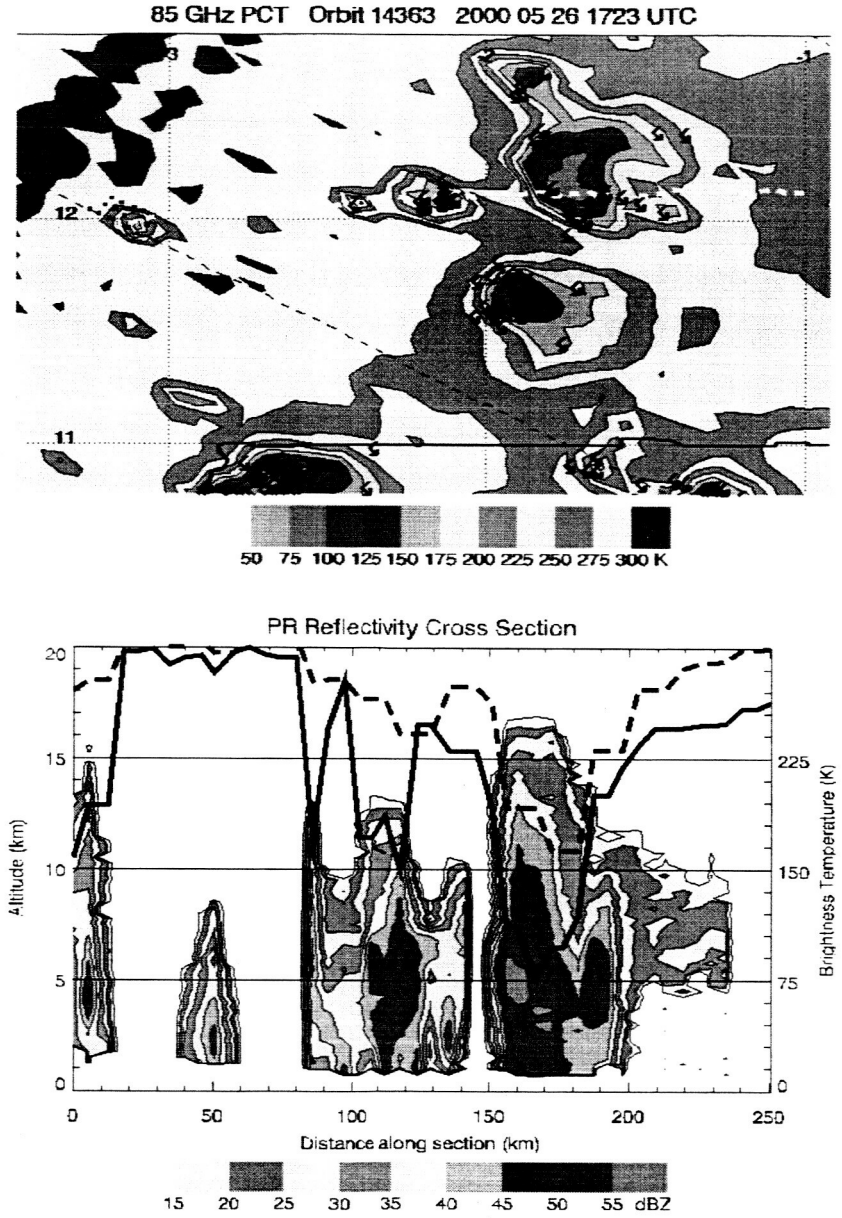

Fig. 14. As in Fig. 11 (different horizontal scale), for precipitation feature over West Africa, 26 May 2000.

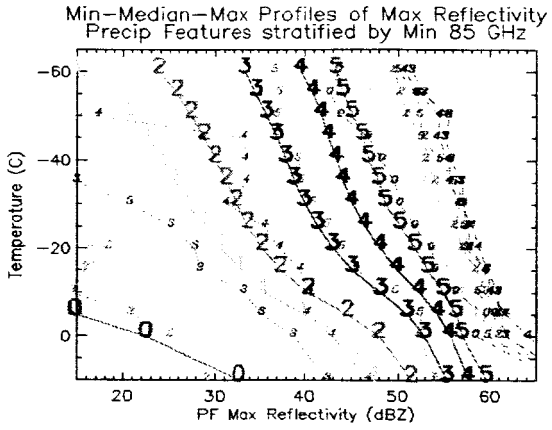

Fig. 15. As in Fig. 9, but stratified by minimum 85-GHz PCT.

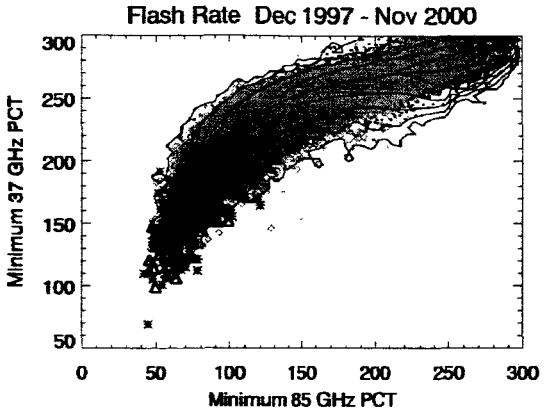

Fig. 16. As in Fig. 10, but with minimum 85-GHz PCT versus minimum 37-GHz PCT. Blue line is the median 37-GHz PCT for each 85-GHz PCT value.

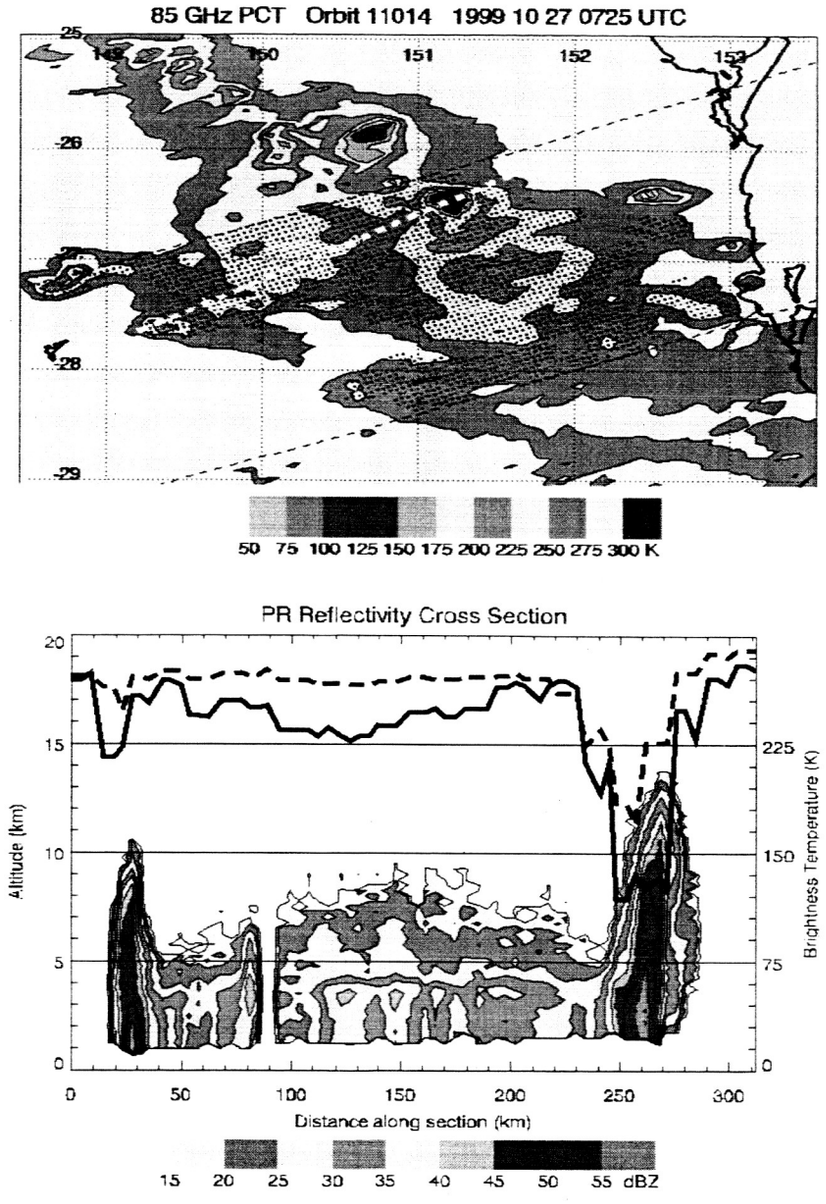

Fig. 17. As in Fig. 11 (different horizontal scale), for precipitation feature west of Brisbane, Australia, 27 Oct 1999. Lightning flash locations omitted for legibility.

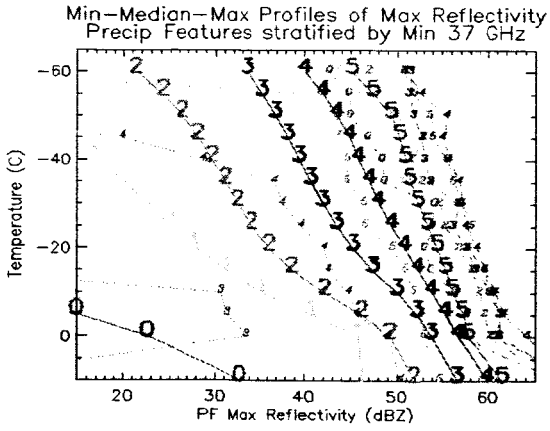

Fig. 18. As in Fig. 9, but stratified by minimum 37-GHz PCT.

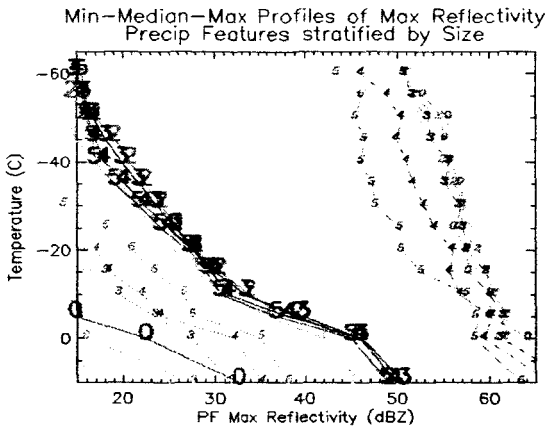

Fig. 19. As in Fig. 9, but stratified by size.

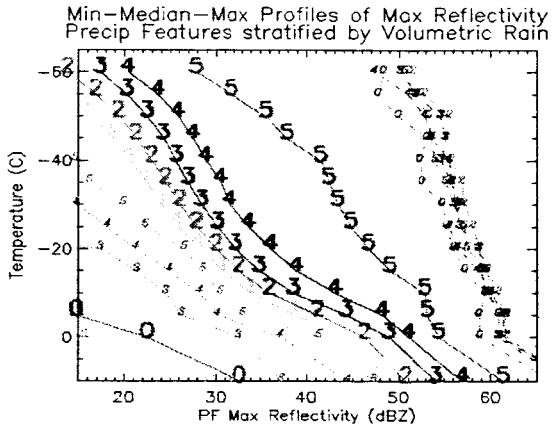

Fig. 20. As in Fig. 9, but stratified by volumetric rain.

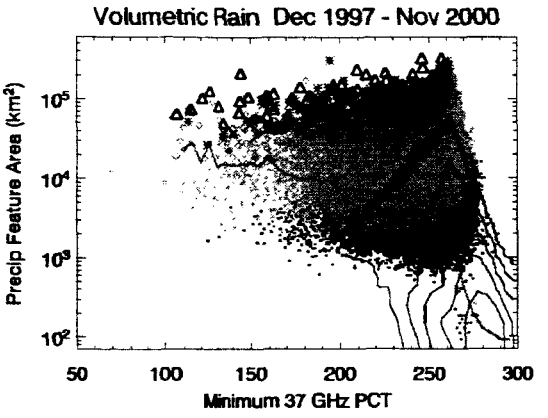

Fig. 21. As in Fig. 10, but with minimum 37-GHz PCT versus size. Symbols correspond to volumetric rain categories one through five.